Nature and distribution of slab-derived fluids and mantle sources beneath the Southeast Mariana forearc rift

Julia M. Ribeiro and Robert J. Stern
Geosciences Department, University of Texas at Dallas, 800 W. Campbell Road, Richardson, Texas, 75083-0688, USA (juliaribeiro@utdallas.edu)

Katherine A. Kelley
Graduate School of Oceanography, University of Rhode Island, Narragansett Bay Campus, Narragansett, Rhode Island, USA

Fernando Martinez
Hawai'i Institute of Geophysics and Planetology, SOEST, University of Hawai'i at Manoa, Honolulu, Hawaii USA

Osamu Ishizuka
Geological Survey of Japan, AIST, Tsukuba, Ibaraki, Japan

Japan Agency for Marine-Earth Science and Technology, Natsushima, Yokosuka, Japan

William I. Manton
Geosciences Department, University of Texas at Dallas, Richardson, Texas, USA

Yasuhiko Ohara
Japan Agency for Marine-Earth Science and Technology, Natsushima, Yokosuka, Japan

Hydrographic and Oceanographic Department of Japan, Koto-ku, Tokyo, Japan

[1] Subduction zone magmas are produced by melting depleted mantle metasomatized by fluids released from the subducted slab. In most subduction zones, formation of backarc basin (BAB) and arc magmas depletes the mantle source toward the trench, resulting in more depleted mantle beneath the forearc. Slab-derived fluids are aqueous beneath the forearc where the slab dehydrates, and the deeper subduction component is increasingly dominated by sediment melt at ≥ 100 km depth. In this study, we present new data for the Southeast Mariana forearc rift (SEMFR), an unusual region of forearc igneous activity, where 2.7–3.7 Ma lavas were recovered by Shinkai 6500 diving and dredged during the TN273 Thomas Thompson cruise. SEMFR is divided into SE (near the trench) and NW (near the arc) sectors. NW SEMFR lavas and glassy rinds are more depleted in melt-mobile elements (e.g., Nb and Yb) and more enriched in fluid-mobile elements (e.g., Cs, Rb, and Ba). SEMFR lavas were produced by partial melting of a BAB-like mantle source, metasomatized by sediment melt and aqueous fluids released from dehydrating the subducted oceanic crust, and the forearc serpentinized peridotites. Evidence of sediment melt, even in SE SEMFR lavas, could be explained by inheritance of BAB-like Th/Nb in the SEMFR mantle source. Geochemical mapping demonstrates that the subduction components and mantle depletion increase towards the arc, suggesting (i) input of a less-depleted mantle beneath SE SEMFR that flowed toward the arc and (ii) aqueous slab-derived fluids become increasingly important at $\sim$50–100 km depth, reflecting that phengite and barite from the downgoing plate and forearc serpentinite broke down beneath the arc volcanoes.

1. Introduction

[2] Subduction zones are places where one hydrated oceanic plate goes underneath another plate, and releases its fluids more or less continuously down to depths of ~200 km or more [*Schmidt and Poli*, 1998]. The subducting slab mostly dehydrates beneath the forearc [*Hacker*, 2008; *Schmidt and Poli*, 1998], so the first fluid released is aqueous. As the slab dehydrates with increasing depth, the slab-derived liquid progressively evolves into hydrous sediment melts at ≥100 km deep (Figure 1) [*Kimura et al.*, 2010; *Manning*, 2004]. Fluid-mobile elements (FMEs: B, Cs, Li, As, Sb, U, Rb, Ba, Sr, K) are carried down by hydrous minerals (e.g., amphibole, biotite, phengite, barite, serpentine, brucite, chlorite), and they are released along with hydrous fluids into the mantle wedge during mineral breakdown [*Hattori and Guillot*, 2003; *Kimura et al.*, 2010; *Plank and Langmuir*, 1998; *Schmidt and Poli*, 1998; *Zack et al.*, 2001]. As subduction proceeds, less FMEs become available from the downgoing plate [*Elliott*, 2003; *Manning*, 2004; *Pearce and Stern*, 2006; *Pearce et al.*, 2005; *Ryan et al.*, 1995], so that aqueous fluids released beneath the forearc are thought to be enriched in FMEs relative to deeper fluids [*Bebout*, 2007; *Bebout et al.*, 1999]. Indeed, studies of serpentinized peridotite clasts from Mariana forearc mud volcanoes and from exposed subduction channel complexes like that of Catalina Island, offshore California, also indicate that shallower fluids are more aqueous (and richer in FMEs) [*Bebout et al.*, 2007; *Fryer et al.*, 2006; *Fryer et al.*, 1995; *Hulme et al.*, 2010; *Savov et al.*, 2007; *Savov et al.*, 2005] than are the deeper fluids [*Kimura et al.*, 2010; *Manning*, 2004; *Pearce et al.*, 2005].

[3] The slab-derived fluids rise up to hydrate and serpentinize the mantle wedge beneath the forearc [*Van Keken et al.*, 2011; *Wada et al.*, 2011] but cause mantle melting at depths ≥100 km beneath the arc and beneath backarc basin (BAB) spreading centers [*Kelley et al.*, 2006; *Kelley et al.*, 2010]. Thus, subduction-related magmas can be understood as partial melts from the hot asthenospheric mantle wedge fluxed by the fluids released from the downgoing plate. As the asthenospheric mantle flows from the backarc basin spreading center toward the trench, the mantle is successively depleted by formation of BAB and arc magmas [*Class et al.*, 2000; *Pearce and Stern*, 2006; *Pearce et al.*, 2005] (Figure 1), resulting in a more depleted mantle beneath the forearc [*Woodhead et al.*, 2012]. Convection of a more depleted mantle toward the trench has been demonstrated by mapping markers of mantle depletion (i.e., Nb/Yb, [*Pearce and Stern*, 2006; *Pearce et al.*, 2005]) and by sampling clasts of forearc peridotites from the Mariana inner trench slope. Such forearc mantle clasts mostly consist of harzburgite, residues of mantle melting [*Ohara and Ishii*, 1998; *Parkinson and Pearce*, 1998; *Savov et al.*, 2007; *Savov et al.*, 2005], which are chemically distinct from the more fertile, BAB peridotites [*Ohara et al.*, 2002].

[4] The Southeast Mariana forearc rift (SEMFR) is an unusual volcanic rift in the Mariana forearc [*Ribeiro et al.*, 2013], which extends from the trench to the southernmost Mariana volcanic arc. Because SEMFR basalts are mantle melts produced beneath the forearc, these potentially provide new insights into shallow subduction zone processes and products (Figure 1). Here, we report the petrography, major and trace element chemistry, and Pb-Nd-Sr radiogenic isotopic compositions for SEMFR mafic lavas to address two major questions: (i) what is the composition of the
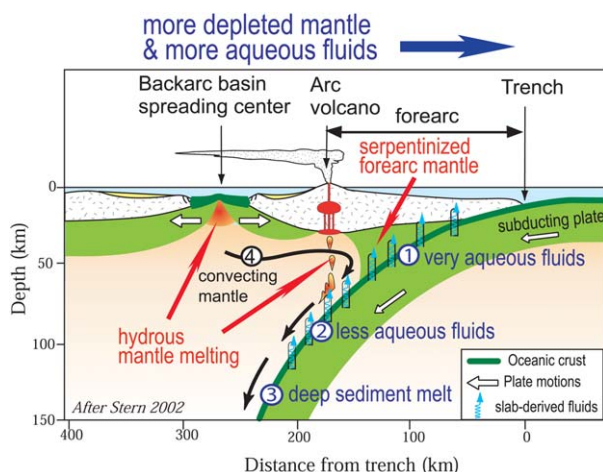
Figure 1. Sketch of a typical subduction zone, after [*Stern*, 2002]. The downgoing plate releases its fluids into the mantle wedge as subduction proceeds. The slab-derived fluid is highly aqueous (water-rich) beneath the forearc (1), and becomes less aqueous with increasing depth (2). The slab-derived fluid becomes a silicate melt from sediment (3) at depth ≥ 100 km. The mantle flows from beneath the backarc basin spreading center toward the trench (4). Formation of magmas beneath the backarc basin, and then beneath the arc, depletes the mantle, resulting in a more depleted mantle toward the trench. Beneath the arc, magmas are produced by melting of a depleted mantle, metasomatized by aqueous fluids and sediment melt; while BAB lavas formed by adiabatic decompression melting of lherzolitic mantle which interacted with deeper, aqueous fluids and hydrous melt from subducted sediment.

mantle source and the slab-derived fluids beneath SEMFR?; and (ii) how do the compositions of the mantle source and the slab-derived fluids vary with slab depth beneath SEMFR?

2. Geodynamic Setting

[5] The southernmost Mariana convergent margin represents the southern end of the Izu-Bonin-Mariana (IBM) intraoceanic arc (Figure 2a). Here, the trench curves from N-S to nearly E-W to accommodate collision of the Caroline Ridge, which began in Late Miocene time [*Miller et al.*, 2006]. This E-W trench segment is also the site of the great Challenger Deep, the deepest point on Earth's solid surface. The subducting slab beneath the southernmost Marianas is able to rollback rapidly because it is short and narrow ($\sim$ 200 km wide, $\sim$ 250 km deep), which triggers upper plate extension and asthenospheric mantle flow beneath the forearc [*Gvirtzman and Stern*, 2004]. These geodynamic conditions result in a rapidly evolving convergent margin, composed of active submarine

arc volcanoes that almost intersect the BAB spreading ridge, the Malaguano-Gadao Ridge (MGR), which lies $\sim$ 110 km from the trench (Figure 2b) [*Fryer et al.*, 1998; *Stern et al.*, 2013]. To the south, MGR almost intersects a caldera with hydrothermal activity [*Gamo et al.*, 2004; *Kakegawa et al.*, 2008], the Toto Caldera, which may be part of the immature magmatic arc [*Ribeiro et al.*, 2013]. This atypical arc – backarc basin configuration allows the backarc mantle of the southernmost Mariana Trough to capture the slab-derived fluids usually released beneath arc volcanoes, enhancing mantle melting to form the inflated MGR [*Becker et al.*, 2010; *Fryer et al.*, 1998], in spite of being a slow-spreading system ($\sim$ 4 cm/yr, [*Kato et al.*, 2003]).

[6] The Eocene forearc [*Reagan et al.*, 2010] has been stretching since Late Neogene time to accommodate opening of the southernmost Mariana Trough, forming SEMFR at 2.7–3.7 Ma by seafloor spreading [*Ribeiro et al.*, 2013]. SEMFR has since evolved into a broadly deformed rift ($\sim$ 40 km wide and at least 60 km long) that overlies the shallow part of the subducting slab ($\leq$50 km deep, [*Becker*, 2005]). SEMFR is traceable from the trench to a complex volcanic arc chain, the Fina Nagu Volcanic Chain (FNVC). Eastward, the SEMFR is bounded by the West Santa Rosa Bank fault (WSRBF; Figure 2b) [*Fryer et al.*, 2003], which overlies a tear in the subducting Pacific plate [*Fryer et al.*, 2003; *Gvirtzman and Stern*, 2004]. In the following, SEMFR is divided into SE (near the trench) and NW (near the arc) sectors, the boundary corresponding to $\sim$ 50 km slab depth (shown by the dashed white line in Figure 2b). SE SEMFR relief (near the trench) is the greatest and the most affected by faulting and landsliding, whereas NW SEMFR (near FNVC) has smoother relief with better-preserved pillow outcrops [*Ribeiro et al.*, 2013].

3. Methods

[7] SEMFR samples were collected in the course of manned submersible (Shinkai 6500) diving (R/V YokosukaYK08-08 Leg 2 and YK10–12 cruises) and dredging (R/V YokosukaYK 10–12 and TN273 Thomas Thompson cruises). We also report trace element contents and Pb-Sr-Nd isotopic compositions of lavas from ROV Kaiko dives 163 and 164 (R/V Kairei KR00–03 Leg 2 cruise). Representative fresh samples were selected for petrographic, geochemical, and isotopic studies. Below we provide a short
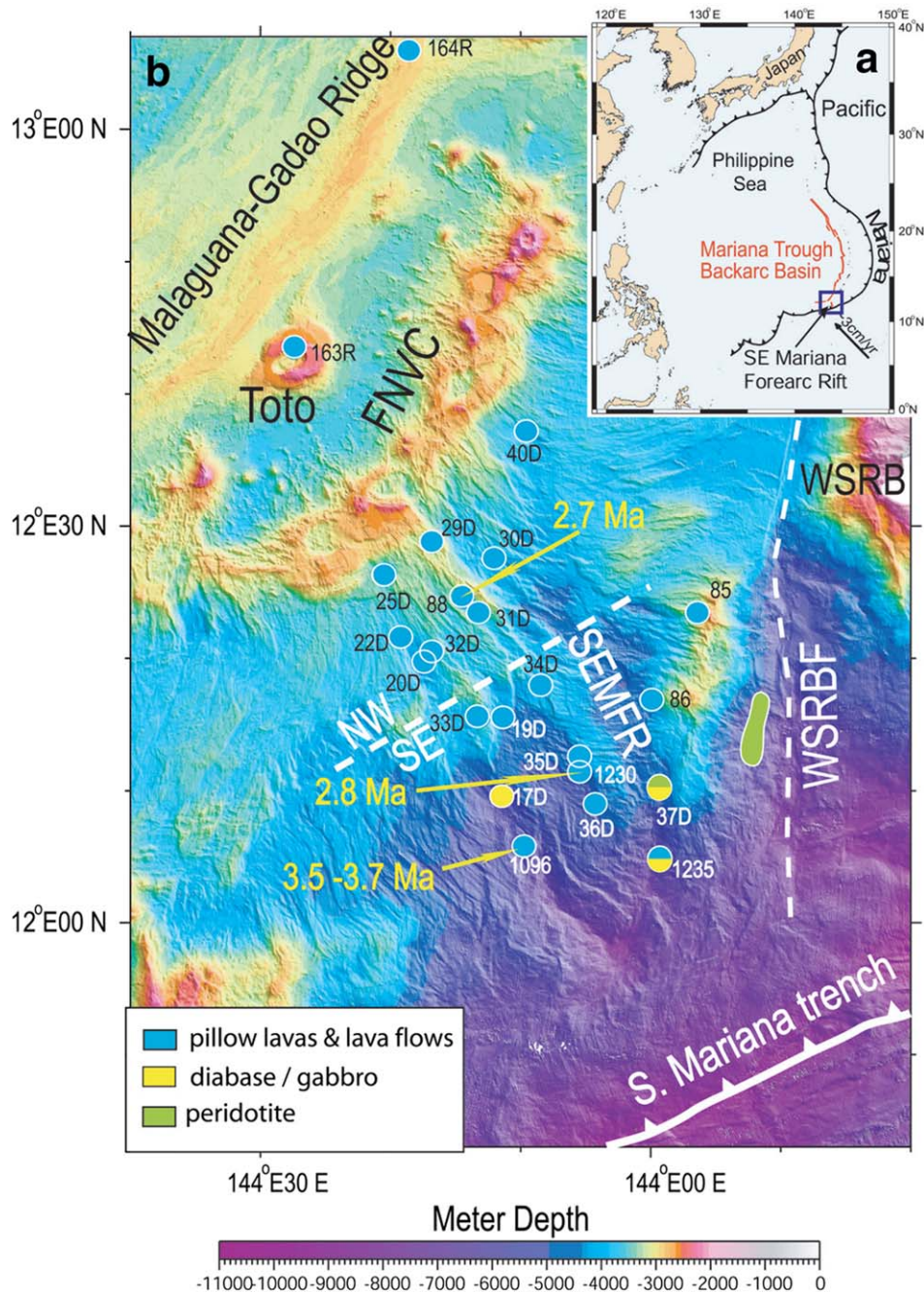
Figure 2. Locality maps. (a) The Mariana intraoceanic arc system. The arrows represent the convergence rates from [*Kato et al.*, 2003]. The blue box shows the area of B. (b) Detailed bathymetric map of the southernmost Mariana intraoceanic arc showing sample sites and their lithologies. The SEMFR is divided in SE and NW sectors, separated by a white dashed line. Map generated with GMT [*Smith and Wessel*, 1990; *Wessel and Smith*, 1995, 1998] using a compilation from the University of New Hampshire / Center for Coastal and Ocean Mapping / Joint Hydrographic Center [*Gardner*, 2006, 2007, 2010]. Toto: Toto Caldera; FNVC: Fina Nagu volcanic chain. Numbers with D indicate TN273 dredging sites, numbers with R are JAMSTEC R/V Karei cruise sampling sites and other numbers represent sampling sites performed during JAMSTEC R/V Yokosuka. The large yellow numbers are ^{40}Ar-^{39}Ar ages for SEMFR lavas. Peridotites (in green) along the West Santa Rosa Bank Fault (WSRBF) are from [*Bloomer and Hawkins*, 1983; *Michibayashi et al.*, 2009; *Sato and Ishii*, 2011].

description for the analytical methods, details are reported in supporting information Appendix A.[1] Major and trace element analyses, and Pb-Sr-Nd isotopic ratios of SEMFR lava whole rocks and glassy rinds are reported in supporting information Tables A1 and A2.

[8] Trace element analyses for dive 1096 (YK08-08 Leg 2 cruise) was carried out at the Geological Survey of Japan (GSJ) [*Ishizuka et al.*, 2009] by ICP-MS (Inductively coupled plasma mass spectrometer) on a VG Platform instrument. Reproducibility is $\leq \pm 4\%$ rsd for REE and $\leq \pm 6\%$ rsd for other trace elements. TN273 samples were analyzed for major element abundances on an Ultima-C Jobin Yvon Horiba Inductively Coupled Plasma Atomic Emission Spectrometry (ICP-AES) at Boston University (BU), and for trace elements on a Thermo X-series II quadrupole ICP-MS at the University of Rhode Island (URI), following the method of [*Kelley et al.*, 2003]. Calibration curves yield $r^2 \geq 0.999$ for trace and major elements, but for P_2O_5 ($r^2 \geq 0.997$). Averaged reproducibility of replicate analyses are <2% rsd for major and trace element analyses, except for P_2O_5 and K_2O (<4% rsd). Major element oxides sum to 100 ± 1 wt % when measuring Fe_2O_3. Sample replicates analyzed by ICP-MS and ICP-AES agree within <4% rsd for TiO_2, Sr and K_2O (Figure A1 in supporting information Appendix A); and trace elements analyzed by ICP-MS in GSJ and at URI agree within <10%.

[9] Fresh, brown, and translucent glass chips from the pillow rinds were polished (Figure A2 in supporting information Appendix A) and analyzed with the Superprobe JEOL JXA-8200 at Massachusetts Institute of Technology (MIT) for major elements, using a 10 μm defocused beam to minimize alkali loss, a 15 kV accelerating voltage and a 10 nA beam current. Repeated analyses of the standard ALV-1690-20 [*Grove et al.*, 1992] gave a mean CaO = 10.85 wt %, Al_2O_3 = 15.51 wt %, K_2O = 0.15 wt %, MnO = 0.19 wt %, Na_2O = 3.13 wt %, TiO_2 = 1.71 wt %, SiO_2 = 49.90 wt %, P_2O_5 = 0.18 wt %, FeO = 9.91 wt %, MgO = 7.68 wt % with a precision <0.3%. Mean of repeated analyses of the unknowns has $1\sigma \leq 0.5\%$. Polished glass chips were ablated with the URI UP-213 Laser Ablation System coupled to a Thermo X-series II quadrupole ICP-MS (LA-ICP-MS) for trace elements, using a 10 Hz repeat rate, 60% pulse beam energy and 80 μm spot size [*Kelley et al.*, 2003]. Data were background-subtracted, and

normalized to ^{43}Ca as internal standard. Calibration curves yield $r^2 \geq 0.999$, but for Li, Be, Y, Lu, and Tm ($r^2 \geq 0.996$). Reproducibility of replicate analyses are $\leq 3\%$ rsd for Sr, Nb, Rb, Ba, K_2O; $\leq 5\%$ rsd for Y, Li, U; and $\leq 11\%$ rsd for Th and Ni. Some glass chips were also dissolved and analyzed by ICP-MS. Agreement between the LA-ICP-MS and the ICP-MS data is $\leq 8\%$ rsd, and agreement between the REE patterns is excellent ($\leq 7\%$ rsd). Major elements analyzed by electron microprobe and by LA-ICP-MS compare well (Figure A3 in Appendix A).

[10] Sample chips were leached with HNO_3 prior to chemical separation for isotopic analyses. Isotopic ratios of Sr, Nd, and Pb were determined using a Finnigan MAT 261 multicollector Thermal Ionization Mass Spectrometer (TIMS) at the University of Texas at Dallas (UTD). Repeated analyses ($n = 15$) of $^{87}Sr/^{86}Sr$ standard (SRM-987) show a mean of 0.71024 ± 3 ($10^{-5} \times 2\sigma$). Repeated measurement ($n = 13$) for La Jolla standard yield ($^{143}Nd/^{144}Nd = 0.51185 \pm 1$ ($10^{-5} \times 2\sigma$)) for Nd mass calibration, and reproducibility of $^{143}Nd/^{144}Nd$ is better than ± 0.00005. Calculations of εNd use the CHUR value ($^{143}Nd/^{144}Nd = 0.512634$) of [*Salters and Stracke*, 2004]. Repeated analyses ($n = 11$) of the standard NBS-981 gave $^{206}Pb/^{204}Pb = 16.895 \pm 0.01$ (2σ), $^{207}Pb/^{204}Pb = 15.435 \pm 0.02$ (2σ), $^{208}Pb/^{204}Pb = 36.515 \pm 0.04$ (2σ) and this was the basis for correcting unknowns for fractionation to the values of [*Todt et al.*, 1996].

[11] Samples were also filtered for alteration. Detailed study of the alteration of SEMFR lavas is reported in supporting information Appendix B. Alteration is not always visible petrographically, and cryptic alteration can affect concentrations of the FMEs in whole rock samples [*Hart*, 1969; *Jochum and Verma*, 1996; *Kelley et al.*, 2003]. Because the FMEs are of special interest in this paper, we selected the freshest whole rock with petrographic alteration $\leq 1\%$. We also report results from glassy rims to further circumvent problems caused by cryptic alteration of whole-rock samples.

4. Results

[12] During R/V YK08-08 Leg 2 and YK10–12 cruises, we mostly collected in SE SEMFR aphyric (<1% phenocrysts) and sparsely phyric (1–5% phenocrysts) microporphyritic pillows or massive lava flows of basalt and basaltic andesite (50.4–
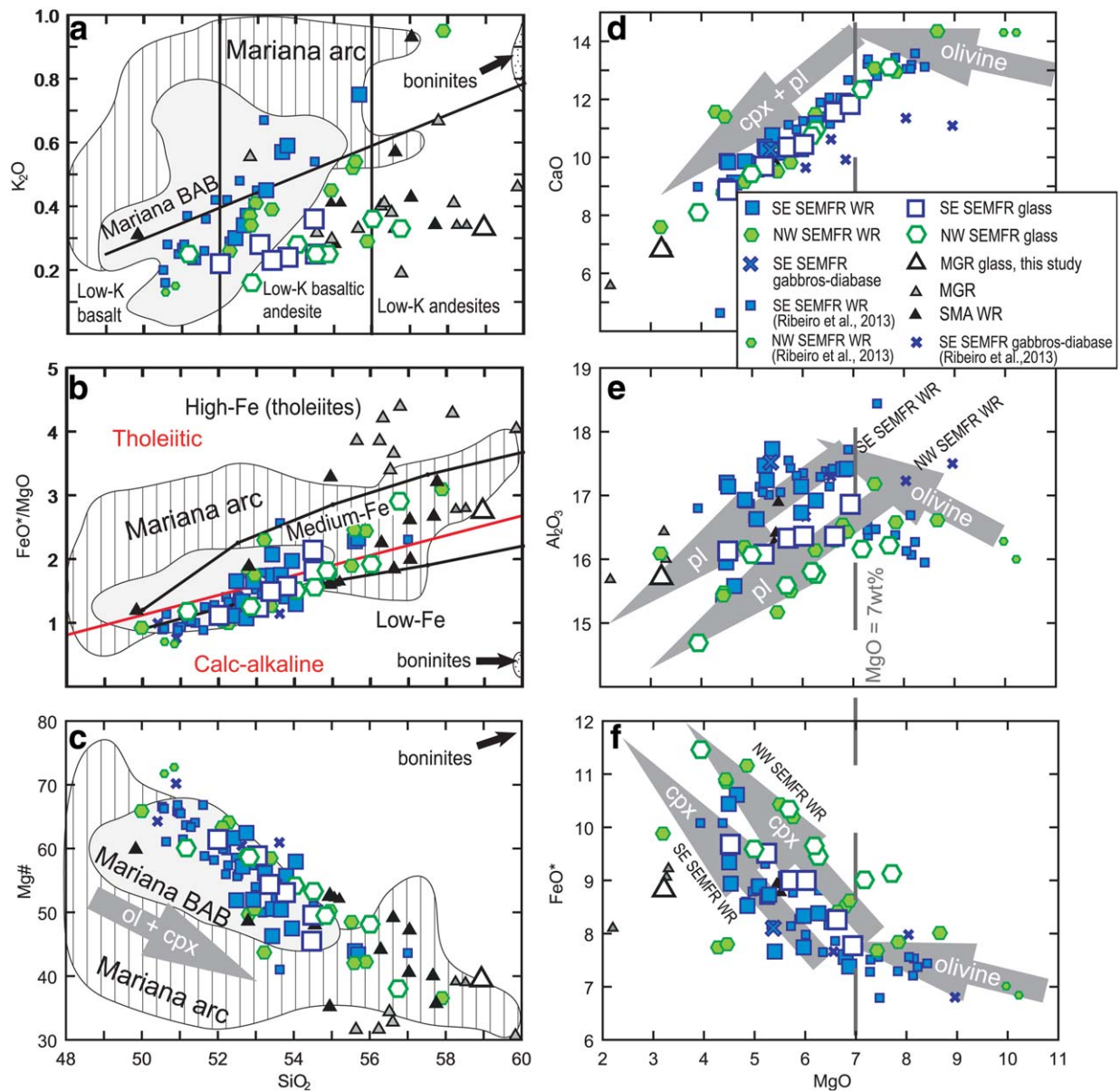
Figure 3. Major element variation diagrams (all data recalculated to 100% anhydrous) for SEMFR lavas. (a) Potassium – silica diagram, with fields after [*Peccerillo and Taylor*, 1976]. Whole rock (WR) samples are filtered for alteration using techniques outlined in supporting information Appendix B. The grey field represents Mariana BAB glassy rinds [*Gribble et al.*, 1996; *Gribble et al.*, 1998; *Hawkins et al.*, 1990; *Ikeda et al.*, 1998; *Kelley and Cottrell*, 2009; *Pearce et al.*, 2005]. Hatched field represents bulk samples from the Mariana arc [*Kelley and Cottrell*, 2009; *Kelley et al.*, 2010; *Kent and Elliott*, 2002; *Pearce et al.*, 2005; *Shaw et al.*, 2008; *Stern et al.*, 2006; *Wade et al.*, 2005]. Small grey triangles denote glassy rinds from the Malaguana-Gadao Ridge (MGR) [*Kakegawa et al.*, 2008; *Pearce et al.*, 2005; *Ribeiro et al.*, 2013; *Stern et al.*, 2013], and small black triangles are data from South Mariana arc whole rock (SMA WR) sampled between 13°10'N–11°N reported in [*Kakegawa et al.*, 2008; *Stern et al.*, 2013], including Toto Caldera samples reported in [*Ribeiro et al.*, 2013]. The field for boninites is from [*Reagan et al.*, 2010]. (b) FeO*/MgO vs SiO₂, after [*Arculus*, 2003]. The red line discriminates between tholeiitic and calk-alkaline lavas [*Miyashiro*, 1974]. (c) Mg# vs SiO₂, (Mg# = 100Mg/(Mg+Fe)), (d) CaO, (e) Al₂O₃, and (f) FeO* vs MgO diagrams for lavas from SEMFR. Arrows represents fractionation trends. The grey dashed line highlights the hinge in CaO, Al₂O₃, and FeO*, resulting from plagioclase and clinopyroxene crystallization starting at MgO = 7 wt %. Pl: Plagioclase, cpx: Clinopyroxene, ol: Olivine. See text for details.

57.0 wt % SiO$_2$, K$_2$O < 1 wt %, Mg# = 41–67). In contrast, NW SEMFR pillow lavas are more primitive, porphyritic basalts (SiO$_2$ < 51 wt %, K$_2$O < 1 wt %, Mg# > 70) that contain larger phenocrysts ($\geq$ 0.5 mm) of clinopyroxene and olivine. Pillow lavas from MGR are vesicular, cryptocrystalline andesites. Lava flows from Toto Caldera are vesicular, sparsely phyric to aphyric, fine-grained to cryptocrystalline basaltic andesites. Detailed petrographic and major element results for SEMFR samples recovered during the R/V Yokosuka and Karei cruises are reported in [*Ribeiro et al.*, 2013]. In this section, we describe the samples recovered from R/V Thomas Thompson TN273 cruise (Figure 2b). Locations of the TN273 dredges are reported in supporting information Table C1; and detailed description of TN273 samples is reported in supporting information Table C2.

4.1. Petrography

[13] SEMFR is mostly floored with fresh pillow lavas and lava flows (Figure 2b) with a thin manganese cover (1–2 mm) and talus slopes of this material. A few plutonic rocks were also recovered during TN273, including olivine – clinopyroxene diabase at dredge 17D, and amphibole gabbros collected along with peridotites at dredge 37D (not studied here). Plutonic rocks are generally more altered than lavas. Diabase, fine-grained gabbros and peridotites were mostly recovered in the easternmost SEMFR (Figure 2b), further demonstrating the importance of faulting and exhumation of the lower crust and upper mantle in that part of the rift [*Michibayashi et al.*, 2009; *Ribeiro et al.*, 2013]. TN273 lavas are mostly fresh to moderately altered, and moderately vesicular basaltic andesites, with few basalts and rare andesite.

[14] Petrography of SEMFR lavas varies along the rift. Lavas from the SE SEMFR are mostly microporphyritic clinopyroxene - plagioclase basalt, with an average of 26% plagioclase, 9% clinopyroxene and ± 1% olivine. NW SEMFR lavas are mostly diabasic and microporphyritic olivine – clinopyroxene – plagioclase basalts, with more plagioclase (31% in average) and clinopyroxene (10% in average), and ± 1% olivine (supporting information Table C2). From the trench to the Fina-Nagu Volcanic Chain (FNVC; Figure 2b), SEMFR lavas are more abundant in plagioclase, clinopyroxene and olivine. This is also reflected by a change in lava texture from microporphyritic to diabasic ($\geq$ 50% crystals, see supporting information Appendix C for details).

4.2. Major Elements

[15] SEMFR lavas (bulk samples and glassy rinds) are low-K to medium-K basaltic andesites, with few basalts and rare andesites (Figure 3a) that cluster along the tholeiitic – calc-alkaline boundary of [*Miyashiro*, 1974] (Figure 3b; low-Fe to medium-Fe in the diagram of [*Arculus*, 2003]). In terms of normative composition, SEMFR lavas are quartz tholeiites (4–20% normative quartz), with no significant difference between NW and SE sectors. In Harker diagrams, SEMFR lavas define a fractionation trend from the most primitive lavas (olivine-rich basalts with Mg# $\sim$ 0.71–0.72 and MgO $\geq$ 8 wt %; see [*Ribeiro et al.*, 2013]) toward MGR andesites (Figures 3c–3e). SEMFR lavas with the highest MgO (> 8 wt %) and low TiO$_2$ (< 0.5 wt %) have low SiO$_2$ ($\sim$ 51 wt %; see [*Ribeiro et al.*, 2013] and Figure 3c), demonstrating that they are not boninites [*Le Bas*, 2000]. Glassy rinds, which represent the quenched melt of submarine basaltic eruptions, plot along the elemental trends of SEMFR whole rocks (Figures 3b–3f). However, glassy rinds have lower Mg#, Al$_2$O$_3$ and higher FeO*/MgO than their host rocks (Figures 3a–3c and 3e), because bulk rocks contain olivine, pyroxene and plagioclase phenocrysts (see Figure B2 in supporting information Appendix B for more details).

[16] Harker variation diagrams (Figures 3c–3f) show that major element contents of SEMFR lavas are controlled by crystal fractionation. SE and NW SEMFR lavas define a single liquid line of descent (LLD) in CaO vs MgO diagram (Figure 3d); but in Al$_2$O$_3$ and FeO* vs MgO diagrams (Figures 3e and 3f), SE and NW SEMFR glassy rinds and whole rocks plot along two distinct LLDs: NW SEMFR lavas have less Al$_2$O$_3$ and more FeO* than those from SE SEMFR. Alternatively, a delay in plagioclase and clinopyroxene crystallization along the LLD, resulting from higher water content in SE SEMFR lavas, could also explain the differences in major elements seen between SE and NW lavas. Indeed, water suppresses clinopyroxene and plagioclase crystallization, shifting the saturation point in Al$_2$O$_3$ and CaO toward lower concentrations [*Sisson and Grove*, 1993]. However, crystallization of clinopyroxene and plagioclase should fractionate CaO and Al$_2$O$_3$ similarly, and we should also observe a delay in the CaO saturation point in the SE lavas relative to the NW lavas. Instead, we observe an enrichment in Al$_2$O$_3$ and depletion in FeO* of SE SEMFR lavas relative to NW lavas,
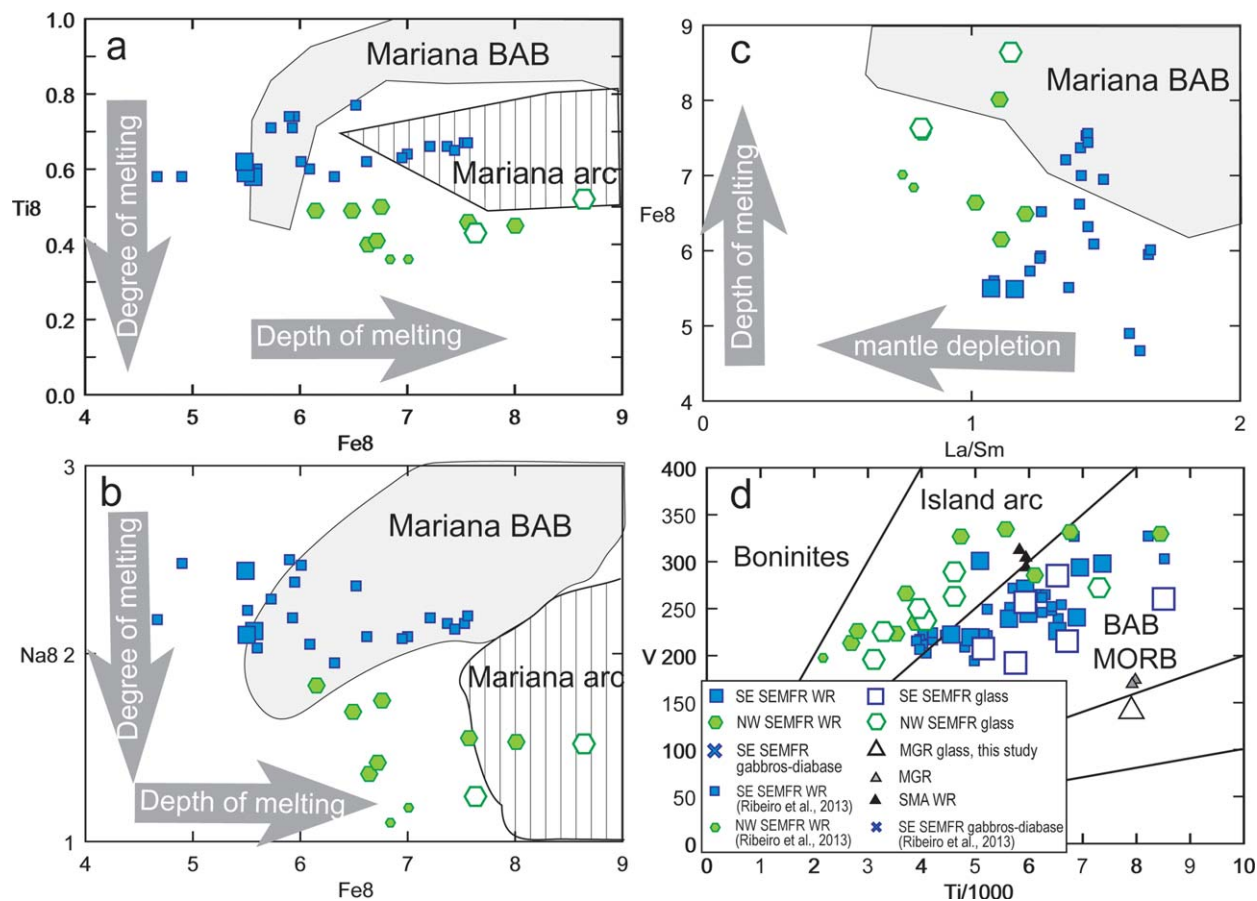
Figure 4. Chemical and magmagenetic variations of NW and SE SEMFR lavas, for both glass and whole rock (WR). (a) Ti_8 vs Fe_8, (b) Na_8 vs Fe_8 and (b) Fe_8 vs La/Sm diagrams. The composition in Na_2O, TiO_2, and FeO of the least fractionated SEMFR lavas (MgO ≥ 7 wt %) were corrected to MgO = 8 wt %. SE SEMFR lavas have higher Ti_8, Na_8, and La/Sm, and lower Fe_8, demonstrating that they were produced from a more enriched mantle source and / or lower degree of mantle melting at shallower depth than NW lavas. (c) Ti-V plot of [*Shervais*, 1982] illustrating the evolution in magmagenetic conditions in SEMFR lavas, from BAB-like decompression melting to arc-like hydrous mantle melting along the rift. See text for details. Small grey triangles denote glassy rinds from the Malaguana-Gadao Ridge (MGR) [*Kakegawa et al.*, 2008; *Pearce et al.*, 2005; *Ribeiro et al.*, 2013; *Stern et al.*, 2013], and small black triangles are data from South Mariana arc whole rock (SMA WR) sampled between 13°10'N and 11°N [*Kakegawa et al.*, 2008; *Stern et al.*, 2013], including Toto Caldera samples reported in [*Ribeiro et al.*, 2013] MORB: mid-ocean ridge basalt.

with no corresponding change in CaO (Figures 3d and 3e), which could reflect a slightly more depleted mantle source for NW SEMFR lavas. Further examination of the major elements and trace elements of the SEMFR lavas (see next paragraph and sections 4.3 and 5.3) also suggests that SEMFR water content and mantle depletion increase toward the NW; and thus, SEMFR geochemical and petrographical variations reflect regional variations in melting processes and/or mantle source along the rift.

[17] To investigate SEMFR magmagenetic processes, lava and glass compositions need to be back-tracked to their compositions as primitive (unfractionated) melts in equilibrium with the mantle [*Kelley et al.*, 2006; *Klein and Langmuir*, 1987; *Langmuir et al.*, 2006; *Taylor and Martinez*, 2003]. The least fractionated rocks (MgO ≥ 7 wt %; Figures 3d–3f), which crystallized only olivine, have been corrected to 8 wt % MgO using the equations of [*Klein and Langmuir*, 1987; *Taylor and Martinez*, 2003] to calculate the Ti_8, Na_8, and Fe_8 contents. TiO_2 and Na_2O are incompatible elements, so Ti_8 and Na_8 reflect the degrees of mantle depletion and mantle melting; whereas Fe_8 tracks the depth of mantle melting [*Klein and Langmuir*, 1987; *Taylor and Martinez*, 2003]. SE
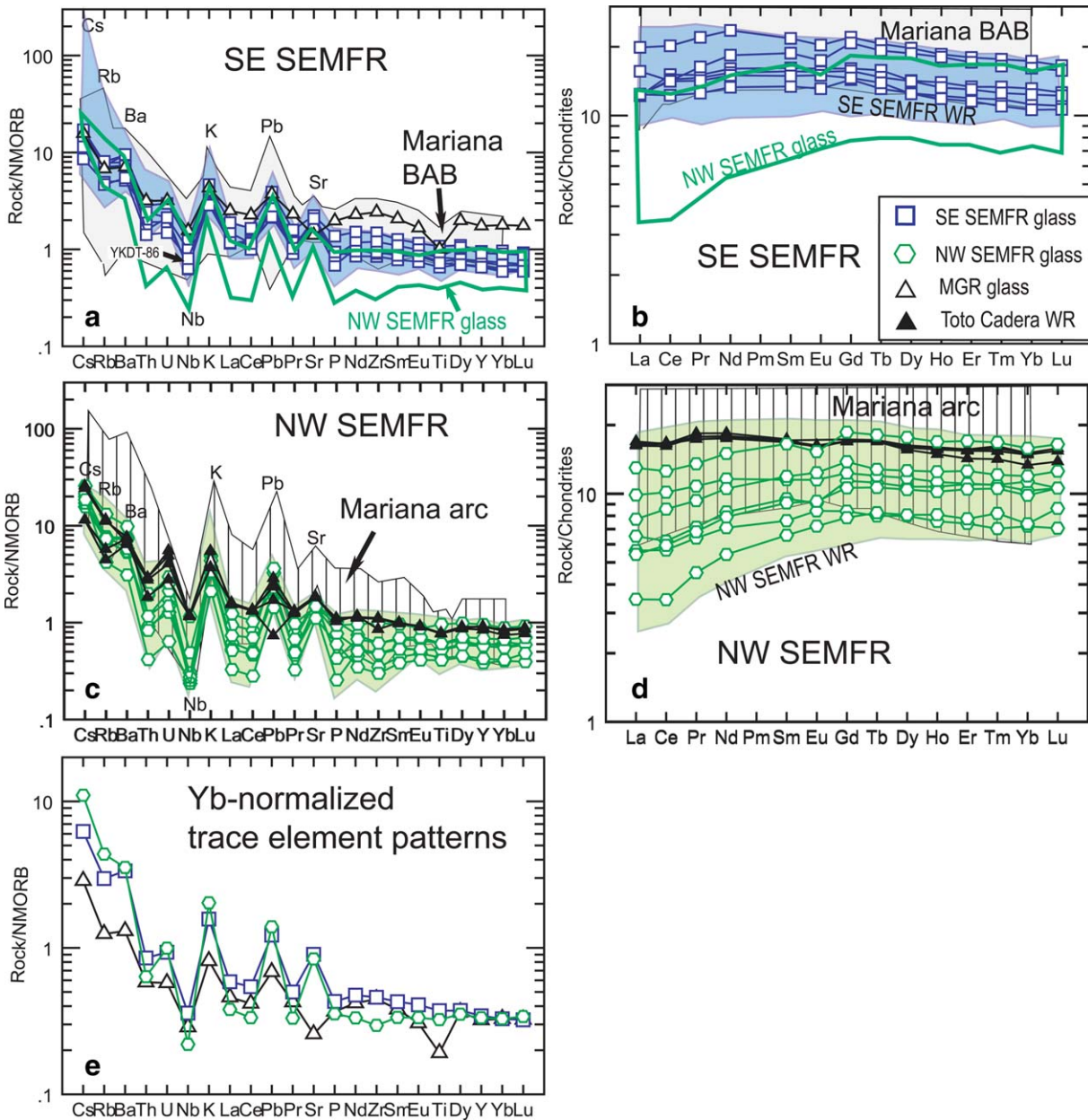
Figure 5. N-MORB normalized [*Sun and McDonough*, 1989] trace element patterns and chondrite-normalized [*Sun and McDonough*, 1989] Rare Earth element (REE) patterns of MGR and SEMFR lavas from the SE sector (a and b) and the NW sector (c and d). SE and NW SEMFR whole rock (WR) are respectively in blue and green fields and they are compared to Mariana arc and BAB lavas. References are reported in caption of Figure 3. (e) Yb-normalized spider diagram for MGR andesite (black triangle), NW SEMFR and SE SEMFR glassy rinds averaged by sector. Glasses are compared to the Toto Caldera whole rock. Note that average NW SEMFR glassy rinds are slightly more enriched in FME/Yb and depleted in HFSE/Yb than are the SE SEMFR glasses.

SEMFR lavas and glass have higher Ti$_8$ and lower Fe$_8$ contents than NW SEMFR lavas, which cluster between Mariana arc and backarc basin compositional fields (Figure 4a). In terms of Na$_8$ and Fe$_8$, SE SEMFR lavas plot within the BAB compositional field (Figure 4b), suggesting that BAB-like

decompression melting of asthenospheric mantle dominated that part of SEMFR. NW SEMFR lavas and glass have lower Ti$_8$ and Na$_8$ at higher Fe$_8$ contents, similar to Mariana arc lavas, suggesting that NW SEMFR lavas were produced deeper and at higher degrees of hydrous mantle melting than

did SE SEMFR lavas [*Kelley et al.*, 2010]. This result also suggests that the magmagenetic conditions of SEMFR lavas evolved from adiabatic decompression melting toward more hydrous mantle melting away from the trench, and SEMFR water content likely increase toward the NW. Differences
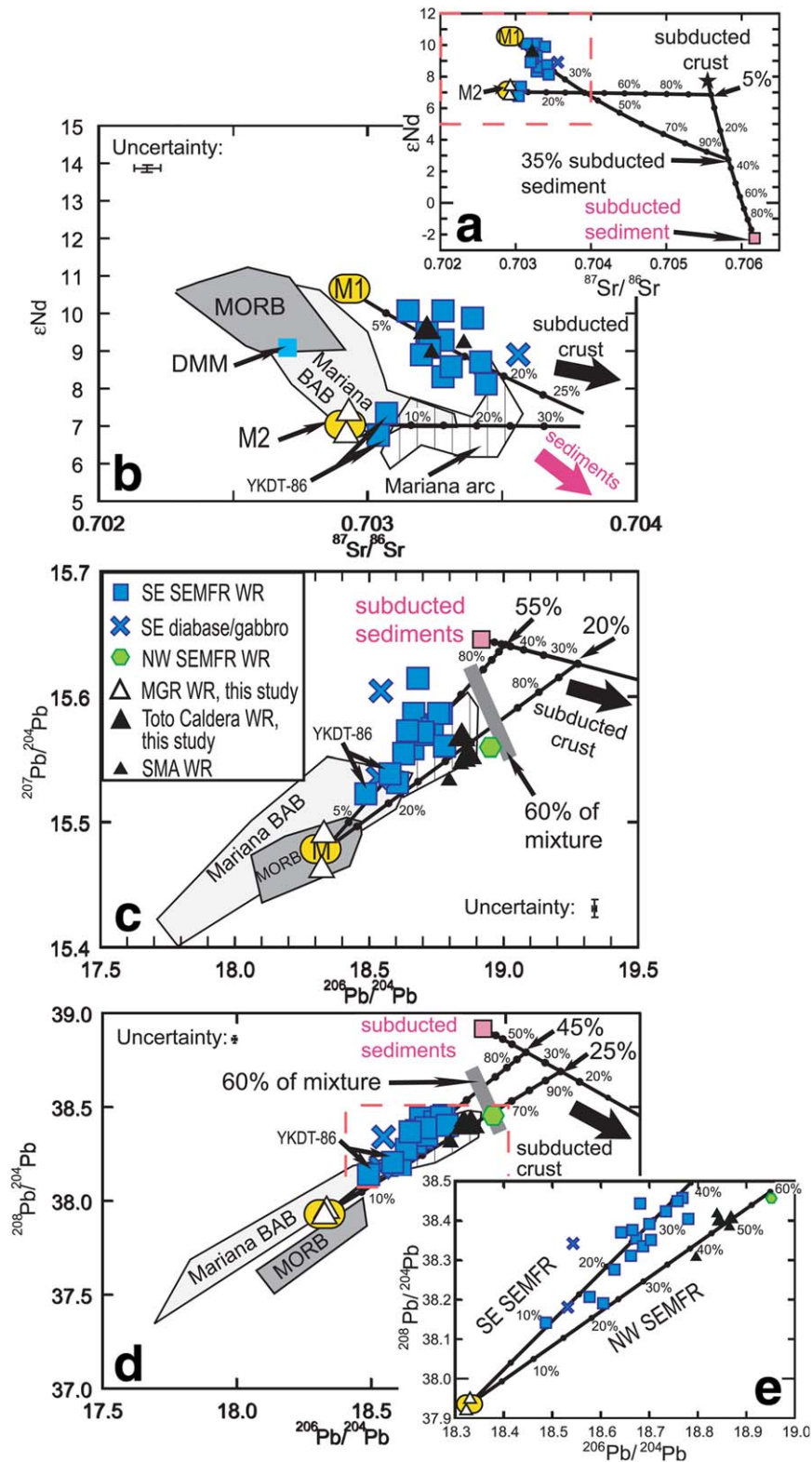

Figure 6.

between the two SEMFR segments are further examined below.

4.3. Trace Elements

[18] Trace elements also provide petrogenetic information about SEMFR lavas. For example, similar to TiO_2 and Na_2O, La, and Sm are melt-mobile elements, with La being more incompatible during mantle melting than Sm. Therefore, La/Sm also tracks the degree of mantle depletion and melting. Plotting Fe_8 against La/Sm (Figure 4c) also demonstrates that NW SEMFR lavas formed deeper from a more depleted mantle source and/or as a result of higher degree of mantle melting than SE SEMFR lavas. Compositional and magmagenetic differences in SEMFR lavas can also be illustrated using the Ti -V plot of [*Shervais*, 1982] (Figure 4d). This diagram combines the melt-mobile behavior of Ti and the sensitivity of V to oxidation state in order to discriminate the tectonic settings of volcanic rocks and ophiolites [*Shervais*, 1982]. Backarc basin lavas are produced by adiabatic decompression of depleted mantle, so that BAB lavas and mid-ocean ridge basalts (MORBs) plot within the same Ti-V compositional field. In contrast, arc lavas formed by melting of a more hydrated and depleted mantle source, shifting the arc compositional field toward lower Ti and higher V (Figure 4d), as reflected by their lower Ti/V relative to BAB lavas [*Reagan et al.*, 2010]. In this diagram, SE SEMFR lavas plot within the BAB compositional field; whereas NW lavas mostly plot within the arc compositional field. These

observations suggest that SEMFR magmagenetic conditions evolved from adiabatic decompression melting to hydrous mantle melting towards the NW, consistent with our previous observations.

[19] Trace element patterns of whole-rock and glass from SEMFR, MGR, and Toto Caldera are typical of subduction-related lavas, with variable enrichments in FMEs (Rb, Ba, Cs, Sr, K, U, and Pb), and depletion in High Field Strength Elements (HFSE: Nb, Zr, Ta, Ti, Rare Earth element (REE), Y), indicating that these melts were derived from a mantle source that was variably depleted and metasomatized by slab-derived fluids (Figure 5). Overall, spider diagrams for SEMFR lavas are similar to those of Mariana arc and backarc basin lavas. Because FME abundances of whole rock samples are easily affected by low degrees of alteration, the following discussion emphasizes the composition of glassy rinds. Trace element patterns of SEMFR glassy rinds show gradually higher HFSE and Th and slightly lower Cs, Rb, and K contents toward the SE (Figures 5a and 5c), as reflected by the lower averages in Cs/Yb, Rb/Yb, K/Yb, and the higher averages in Nb/Yb, Ti/Yb, LREE/Yb in the SE SEMFR glasses relative to the NW SEMFR glasses (Figure 5e). Trace element patterns of MGR lavas are similar to Mariana BAB basalts (Figure 5a). In addition, their less incompatible elements and REE abundances are elevated relative to those of SE SEMFR lavas (Figure 5c). Trace elements patterns of Toto Caldera lavas are similar to those of Mariana arc and NW SEMFR lavas. REE patterns of SE SEMFR whole rock (WR) and glassy rinds

Figure 6. Nd-Sr-Pb isotopic compositions of SEMFR lavas. (a) εNd vs $^{87}Sr/^{86}Sr$ diagram. The red square highlights the area of b. (b) εNd vs $^{87}Sr/^{86}Sr$ diagram focusing on the upper left part of the panel A. Samples from YDKT-86 and the rest of the SE SEMFR lavas have different εNd composition with similar $^{87}Sr/^{86}Sr$, suggesting that an enriched mantle M1 (εNd = 10.65, $^{87}Sr/^{86}Sr$ = 0.70293) and a more depleted mantle M2 (εNd = 7.04, $^{87}Sr/^{86}Sr$ = 0.70293) mixed beneath SE SEMFR. εNd composition of M1 is assessed from the trend observed for most of the SE SEMFR lavas. εNd and $^{87}Sr/^{86}Sr$ composition of M2 and $^{87}Sr/^{86}Sr$ composition of M1 are estimated from MGR whole rock (WR) composition. $^{207}Pb/^{204}Pb$ (c) and $^{208}Pb/^{204}Pb$ (d) vs $^{206}Pb/^{204}Pb$ diagrams. The red rectangle shows the area of E. (e) $^{208}Pb/^{204}Pb$ vs $^{206}Pb/^{204}$ diagram highlighting the compositional variation of SEMFR lavas. The thick black lines with dots are mixing arrays between aBAB-like mantle source M ($^{207}Pb/^{204}Pb$ = 15.48, $^{208}Pb/^{204}$ Pb = 37.93, $^{206}Pb/^{204}Pb$ = 18.33, yellow field) that encompasses the composition of M1 and M2, an averaged Pb-Sr-Nd composition of the altered Pacific oceanic crust (black star) of [*Hauff et al.*, 2003], and a mixture of the Pacific sediments from the ODP site 800 and 801 (pink square) of [*Plank and Langmuir*, 1998]. Numbers represent percentages between the end-members. See Table D1 in supporting information Appendix D for details about the composition of the end-members. The mixing arrays were calculated assuming bulk mixtures. We also plotted the bulk composition of the depleted MORB-type mantle (DMM) of [*Salters and Stracke*, 2004], the Pacific and Atlantic MORBs of [*Chauvel and Blichert-Toft*, 2001], the Mariana arc lavas of [*Stern et al.*, 2006; *Wade et al.*, 2005; *Woodhead*, 1989], the Mariana backarc basin lavas of [*Gribble et al.*, 1998; *Gribble et al.*, 1996; *Volpe et al.*, 1987; *Volpe et al.*, 1990], and the South Mariana arc lavas (SMA) [*Stern et al.*, 2013]. We used the whole rock (WR) composition of the lavas, analyzed by TIMS and ICP-MS, to observe their compositional variations, as more bulk rocks were analyzed.
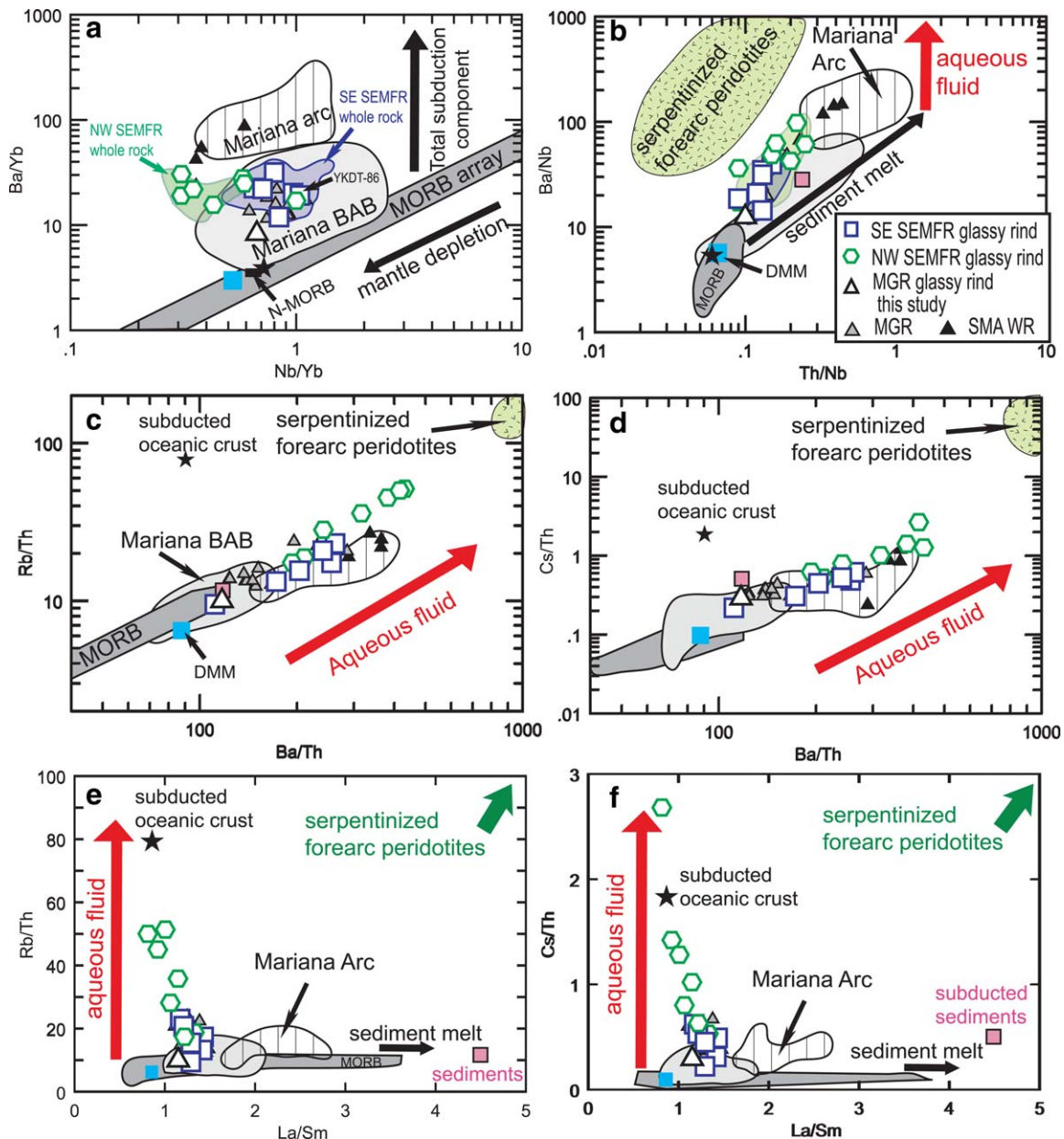
Figure 7. Geochemical proxies used to discriminate subduction and mantle components for SEMFR lavas and related rocks, after [*Elliott*, 2003; *Pearce et al.*, 2005]. (a) Ba/Yb vs Nb/Yb discriminates the total subduction component (Ba/Yb) from mantle depletion (Nb/Yb). NW SEMFR lavas have lower Nb/Yb and slightly higher Ba/Yb than SE SEMFR lavas. (b) Ba/Nb vs Th/Nb diagram is used to discriminate the deep sediment melt from the aqueous fluid. Stronger Ba/Nb in NW SEMFR lavas and in the serpentinized peridotites from South Chamorro seamount in the Mariana forearc [*Savov et al.*, 2007], relative to arc lavas and BAB lavas, reflect the role of an aqueous fluid (red arrow) released beneath the forearc. Compositions of the whole rock (WR) are represented by a green field for NW SEMFR and a blue field for SE SEMFR. Note that compositions of the NW and SE SEMFR glassy rinds and whole rock match. Rb/Th (c) and Cs/Th (d) vs Ba/Th diagrams used to characterize the composition of the aqueous fluid. NW SEMFR glassy rinds have higher Cs/Th and Rb/Th than SE SEMFR, arc and BAB lavas. We used a mixture of the ODP site 800 and 801 Pacific sediments of [*Plank and Langmuir*, 1998] for the subducted sediments (pink square), and a mixture of the altered Pacific oceanic crust of [*Kelley et al.*, 2003] for the subducted oceanic crust (black star). Plots of Rb/Th (e), and Cs/Th (f) vs La/Sm to identify the sources of the aqueous fluid. The MORB compositional field (in grey) is from [*Jenner and O'Neill*, 2012; *Pearce et al.*, 2005]. Small grey triangles denote glassy rinds from the Malaguana-Gadao Ridge (MGR) [*Kakegawa et al.*, 2008; *Pearce et al.*, 2005; *Stern et al.*, 2013], and small black triangles are data from South Mariana arc whole rock (SMA WR) sampled between 13°10'N and 11°N [*Kakegawa et al.*, 2008; *Stern et al.*, 2013]. See text for more details.

are nearly flat, although slightly humped in MREE ($(La/Yb)_N \sim 1$; $(La/Sm)_N \sim 1$; $(Gd/Yb)_N \sim 1$), with no europium anomaly ($(Eu/Eu^*)_N \sim 1$), and they are similar to REE patterns of Mariana BAB lavas (Figure 5b) [*Gribble et al.*, 1998; *Gribble et al.*, 1996; *Hawkins et al.*, 1990; *Ikeda et al.*, 1998; *Kelley and Cottrell*, 2009; *Pearce et al.*, 2005]. In contrast, NW SEMFR WR and glass have more strongly LREE-depleted (N-MORB-like) patterns ($(La/Yb)_N = 0.5–1$; $(La/Sm)_N = 0.5–1$; $(Gd/Yb)_N \sim 1$; $(Eu/Eu^*)_N \sim 1$; Figure 5d), and they have more arc-like trace element patterns. These observations suggest that the degree of mantle melting, mantle depletion and the input of aqueous slab-derived fluids increase toward the NW, consistent with inferences from the Na8, Ti8, Fe8 and Ti-V plots.

4.4. Nd, Sr, and Pb Isotopic Compositions

[20] Radiogenic isotopes are not fractionated during magmatic processes, they are thus commonly used to identify reservoirs. Nd is a melt-mobile element that tracks the mantle wedge. Sr and Pb are mobilized with aqueous fluids and silicate melts, and they track the mantle and the subduction components. SE SEMFR lavas show homogeneous Sr and Nd isotopic compositions (Figures 6a and 6b), with a mean of $^{87}Sr/^{86}Sr = 0.70333 \pm 1$ ($2\sigma \times 10^{-5}$), $^{143}Nd/^{144}Nd = 0.51308 \pm 4$ ($2\sigma \times 10^{-5}$), and $\varepsilon Nd = 8.8 \pm 0.8$. Only YKDT-86 samples have Nd-Sr isotopic compositions that differ, with $^{87}Sr/^{86}Sr$ (mean $^{87}Sr/^{86}Sr = 0.70306 \pm 1$) and lower $^{143}Nd/^{144}Nd$ (mean $= 0.51300 \pm 1$, $\varepsilon Nd = 7.0 \pm 0.2$) similar to MGR lavas (mean $^{87}Sr/^{86}Sr = 0.70293 \pm 0.4$, $^{143}Nd/^{144}Nd = 0.51301 \pm 1$, $\varepsilon Nd = 7.3 \pm 0.2$), suggesting that the mantle wedge beneath YKDT-86 dredge site is more depleted (Figure 6b). However, such variations are not reflected in the trace element patterns and in the Pb-Sr isotopic composition of SE SEMFR lavas, and their Nb/Yb (also tracking mantle depletion) plot homogeneously within the BAB and SE SEMFR compositional fields (Figure 7a). SE SEMFR and Toto Caldera lavas are offset to higher $^{87}Sr/^{86}Sr$ compared with Mariana BAB lavas [*Gribble et al.*, 1998; *Gribble et al.*, 1996; *Volpe et al.*, 1987; *Volpe et al.*, 1990], demonstrating higher contribution from the subducting plate beneath SEMFR (Figures 6a and 6b). SEMFR lavas have εNd that is similar to that of Mariana BAB lavas [*Stern et al.*, 2006; *Wade et al.*, 2005; *Woodhead*, 1989], suggesting a BAB-like mantle source.

[21] Pb isotopic compositions of SEMFR lavas are similar to Mariana arc lavas (mean

$^{206}Pb/^{204}Pb = 18.67 \pm 0.01$ (2σ), $^{208}Pb/^{204}Pb = 38.34 \pm 0.01$ (2σ), $^{207}Pb/^{204}Pb = 15.57 \pm 0.001$ (2σ)), and they define a linear array from Mariana BABB toward subducted Pacific sediment [*Plank and Langmuir*, 1998], further demonstrating that sediments are important in the SEMFR subduction component (Figures 5c–5e). MGR lavas are distinctly less radiogenic than those of SEMFR lavas (mean $^{206}Pb/^{204}Pb = 18.32 \pm 0.03$, $^{208}Pb/^{204}Pb = 37.92 \pm 0.01$, $^{207}Pb/^{204}Pb = 15.46 \pm 0.01$), and they plot within the BAB compositional field, consistent with a less pronounced subduction signature in the MGR lavas. Toto Caldera lavas (mean $^{206}Pb/^{204}Pb = 18.86 \pm 0.01$, $^{208}Pb/^{204}Pb = 38.40 \pm 0.002$, $^{207}Pb/^{204}Pb = 15.56 \pm 0.005$) cluster in the arc compositional field, near the NW SEMFR lavas, also suggesting that arc-like magmagenetic conditions occurred towards the NW.

5. Discussion

[22] SEMFR formed $\sim$ 2.7–3.7 Ma ago by stretching of pre-existing SE Mariana forearc lithosphere to accommodate opening of the MGR backarc basin spreading center. These conditions allowed asthenospheric mantle to flow along SEMFR, resulting in a BAB-like mantle wedge, fluxed by the slab-derived fluids/melts, that melted by adiabatic decompression at $\sim 23 \pm 6.6$ km depth and $1239 \pm 40^o C$ [*Lee et al.*, 2009; *Ribeiro et al.*, 2013]. Beneath the Mariana intraoceanic arc, the subduction components generally consist of aqueous fluids and sediment melts released from the downgoing plate [*Elliott*, 2003; *Pearce et al.*, 2005]. Mantle and subduction components are characterized by different incompatible trace element ratios [*Elliott*, 2003; *Pearce*, 2008; *Plank and Langmuir*, 1998] and different Pb-Sr-Nd isotopic ratios [*Class et al.*, 2000; *Escrig et al.*, 2009; *Stern et al.*, 2006]. By combining these elemental differences, we can (i) test the hypothesis that SEMFR lavas formed from a BAB-like mantle source, (ii) examine the nature and the evolution of the mantle and subduction components beneath SEMFR, and (iii) unravel the different contributions from the downgoing sediments and oceanic crust as aqueous fluids or silicate melts in SEMFR lavas.

5.1. Nature of the Mantle and Subduction Components

[23] The SEMFR mantle and subduction components can be tracked by using trace element

ratios and Nd-Pb-Sr isotopic composition of the lavas. Ratios of fluid-mobile elements (e.g., Ba, Rb, Cs) and melt-mobile elements (e.g., Th, Pb, La) over a less incompatible, fluid-immobile element (e.g., Ce, Nd, Sm, HFSE, HREE) are corrected for fractionation and melting processes and track only the mantle and/or the subduction components [*Elliott*, 2003; *McCulloch and Gamble*, 1991; *Pearce et al.*, 2005].
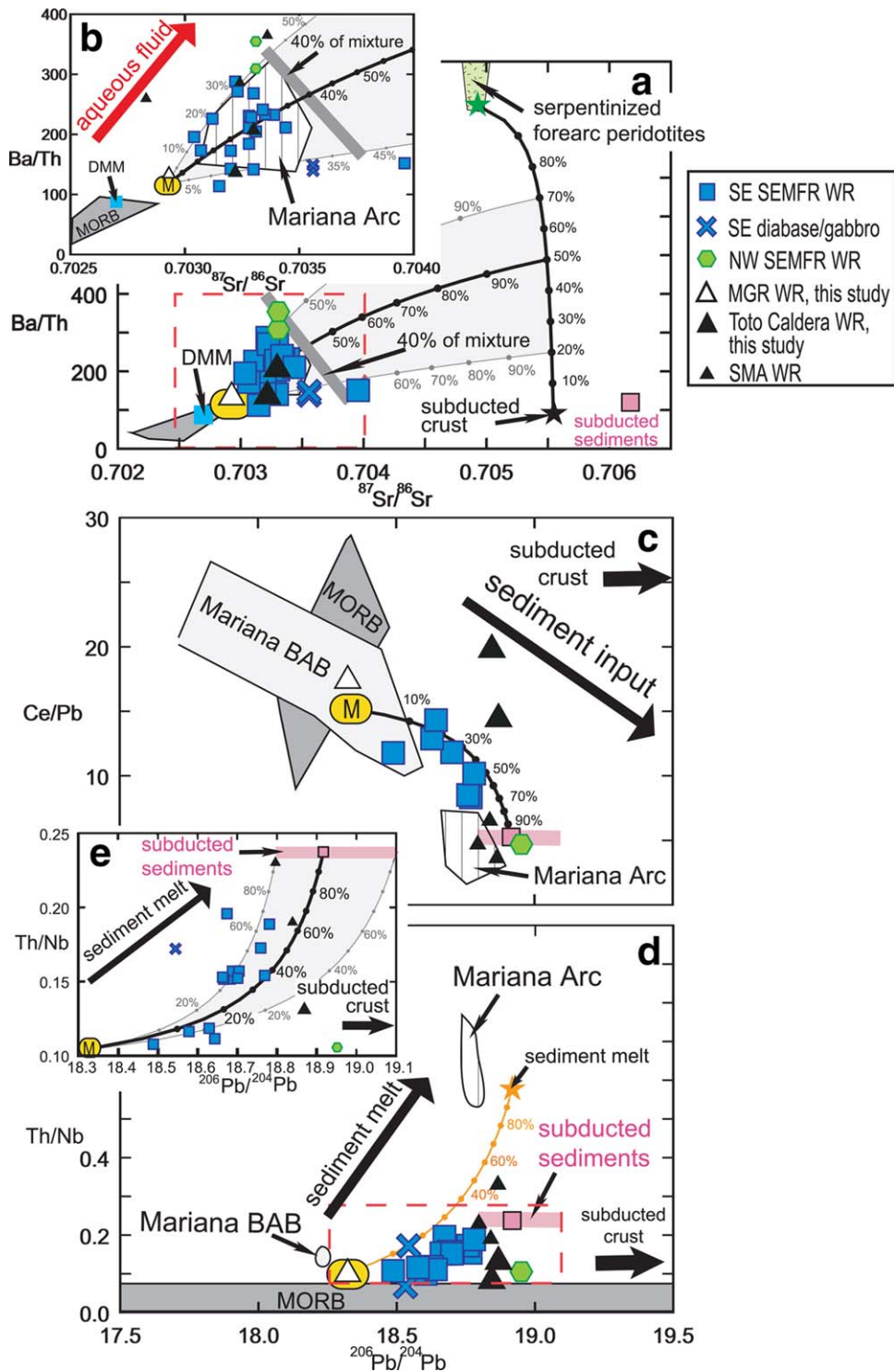

Figure 8.

[24] The ratios of a strongly melt-mobile element over a slightly melt-mobile element (i.e., Nb/Yb) can be used to characterize mantle fertility. Low Nb/Yb (<1) in Mariana arc lavas reflects a depleted BAB mantle source from which BAB melts were previously extracted [*Kelley et al.*, 2006; *Pearce et al.*, 2005]. SEMFR lavas have BAB-like Nb/Yb (= 0.3–1.0, Figure 7a) consistent with their Nd isotopic ratios (averaged εNd = 8.6 $\pm$ 0.1), demonstrating their BAB-like mantle source (Figures 6a–b and 7a). Composition of the SEMFR mantle source is defined by sample showing minimal subduction input. We used an averaged composition of the MGR glassy rinds (analyzed by LA-ICP-MS and TIMS) to estimate the Pb-Sr isotopic and trace element compositions of the SEMFR mantle wedge, as MGR lavas have the lowest contribution in subduction components (Figures 6–8). εNd of the SEMFR mantle wedge was assessed from the trend formed by the SE SEMFR lavas and the South Mariana arc (SMA) lavas in the diagram εNd vs ^{87}Sr/^{86}Sr (Figure 6b). NW SEMFR lavas have arc-like chemical signatures in major elements, trace elements and Pb-Sr isotopic ratios similar to those of the SMA arc lavas (Figures 5–8), as they formed under similar magmagenetic conditions. Thus, we estimated the composition of NW SEMFR endmembers from the trends formed by NW SEMFR lavas and SMA lavas (Figures 6c-e). Based on these estimations, the SEMFR mantle wedge has a BAB-like composition, with εNd = 10.65, ^{87}Sr/^{86}Sr = 0.70293 and ^{206}Pb/^{204}Pb = 18.33. Only YKDT-86 samples derived from a more depleted mantle wedge, with εNd = 7.04 estimated from the MGR εNd bulk composition, suggesting mixing of depleted and enriched mantle beneath SEMFR. Estimated iso-topic and trace element compositions of SEMFR mantle and subduction components are reported in details in supporting information Table D1.

[25] To discriminate between aqueous fluids and silicate melts in the SEMFR subduction components, we can use trace element ratios. Ratios of a slab-derived fluid/melt-mobile element (i.e., Ba, Cs, Rb, Th, La) over a slab-derived fluid-immobile element (i.e., Nb, Ta, Yb, Sm) are good proxies to track subduction components [*Pearce et al.*, 2005]. For example, Ba, Rb, and Cs migrate with the aqueous fluids [*McCulloch and Gamble*, 1991] and with the deeper sediment melt [*Manning*, 2004; *Pearce et al.*, 2005]; while Th and La are only mobilized with sediment melts [*Johnson and Plank*, 1999]. Therefore, Ba/Yb and Ba/Nb track the total subduction component, Th/Nb and La/Sm track the deep sediment melt, and Ba/Th, Rb/Th and Cs/Th track the shallower aqueous fluids [*Elliott*, 2003; *Pearce et al.*, 2005] (Figure 1). SEMFR lavas have BAB-like Ba/Yb ($\leq$ 40), plotting well above the MORB array of [*Jenner and O'Neill*, 2012; *Pearce et al.*, 2005] (Figure 7a), reflecting the SEMFR subduction component. In Ba/Nb vs Th/Nb diagrams (Figure 7b) of [*Pearce and Stern*, 2006], the compositional field of Mariana BAB lavas [*Gribble et al.*, 1998; *Gribble et al.*, 1996; *Hawkins et al.*, 1990] reflects the contribution of deep sediment melt; whereas enrichment of Ba without any enrichment in Th defines the shallower aqueous fluid [*Pearce and Stern*, 2006; *Pearce et al.*, 2005]. Mariana arc lavas [*Fryer*, 1993; *Kakegawa et al.*, 2008; *Pearce et al.*, 2005; *Stern et al.*, 2006; *Stern et al.*, 2013; *Wade et al.*, 2005] are enriched in aqueous fluid and deep sediment melt. SE SEMFR lavas plot within the Mariana BAB composition field; whereas

Figure 8. (a) Ba/Th vs ^{87}Sr/^{86}Sr diagram tracking the sources of the slab-derived fluids captured by SEMFR lavas. The red rectangle shows the area of B. (b) Ba/Th vs ^{87}Sr/^{86}Sr diagram highlighting the compositional variations of SEMFR lavas. The compositional range of SEMFR lavas are modeled by a mixing array between the mantle source (M, ^{87}Sr/^{86}Sr = 0.70293, Ba/Th = 0.10), the forearc serpentinites (^{87}Sr/^{86}Sr = 0.70492, Ba/Th = 888.9, green star, [*Savov et al.*, 2007]), and an averaged of the subducted oceanic crust of [*Hauff et al.*, 2003; *Kelley et al.*, 2003]. Ce/Pb (c) and Th/Nb (d) vs ^{206}Pb/^{204}Pb diagrams tracking the composition of the sediment inputs (fluid/melt phase) captured by SEMFR lavas. The red rectangle highlights the area of e. (e) Th/Nb vs ^{206}Pb/^{204}Pb diagram constraining the composition of sediment melt released beneath SEMFR. Mixing array between the mantle wedge M (^{206}Pb/^{204}Pb = 18.33, Ce/Pb = 15.22, Th/Nb = 0.10) and an arc-like sediment melt (Th/Nb = 0.58, ^{206}Pb/^{204}Pb = 18.92, orange star) in thin orange line misses the SEMFR compositional array. Composition of M is estimated from MGR whole rock (WR) composition for the Pb-Nd-Sr isotopic ratios and from MGR glassy rind composition for the trace elements. SE SEMFR compositional range is explained by a mixture between the mantle source and the subducted Pacific sediment of [*Plank and Langmuir*, 1998]. Detailed composition of the end-members is reported in Appendix Table D1. The ^{206}Pb/^{204}Pb isotopic compositions of the Pacific sediments do not explain the compositional range in ^{206}Pb/^{204}Pb observed in SE SEMFR lavas. We suspect that ^{206}Pb/^{204}Pb isotopic composition of the Pacific sediments subducting beneath SEMFR ranges from 18.8 to 18.91, as shown by the thick pink line. South Mariana arc lavas (SMA, [*Stern et al.*, 2013]) are represented by smaller black triangles.

NW SEMFR lavas have higher Ba/Nb (Figure 7b), demonstrating that the aqueous fluid signal increases away from the trench. The BAB-like Th/Nb and La/Sm in SEMFR lavas suggests interaction of their mantle source with a sediment melt (Figures 7b, 7e, and 7f). This signature perhaps results from inheritance of BAB-like Th/Nb and La/Sm ratios from the SEMFR mantle source.

[26] Trace element systematics similar to the approach of [*Pearce and Stern*, 2006; *Pearce et al.*, 2005] can be applied by using Cs and Rb in order to investigate the composition of the SEMFR aqueous fluids. For this, we must avoid cryptically altered whole rocks and rely on glassy rims. We use the ratios Cs/Th, Ba/Th and Rb/Th to better distinguish shallow aqueous inputs from the deep sediment melt component. In Figures 7c–7f, SE SEMFR lavas plot along the arc compositional field, while NW SEMFR lavas have higher Rb/Th and Cs/Th than arc and BAB lavas. These results demonstrate that (i) the mantle source of SEMFR lavas captured an aqueous fluid and (ii) the mantle source of NW SEMFR lavas interacted with an aqueous fluid that was richer in Ba, Rb, and Cs than the fluid released beneath the arc and the backarc basin spreading center. This enrichment in FMEs in SEMFR lavas suggests that the SEMFR mantle captured the aqueous fluids released from the shallow part of the downgoing plate.

5.2. Sources of the Slab-Derived Fluids and Melts Beneath SEMFR

[27] Subduction-related magmas form from partial melting of the hot asthenospheric mantle wedge fluxed by fluids/melts released from the downgoing plate (Figure 1). However, the serpentinized forearc mantle can also play a role in geochemical recycling of such magmas, as it formed by alteration of the cold mantle wedge metasomatized by the slab-derived fluids released beneath the forearc [*Deschamps et al.*, 2011; *Fryer et al.*, 2006; *Pabst et al.*, 2011; *Pabst et al.*, 2012; *Scambelluri and Tonarini*, 2012]. Therefore, three sources can be considered for the slab-derived fluids/melts released beneath SEMFR: (i) subducted altered oceanic crust [*Elliott*, 2003; *Kelley et al.*, 2003]; (ii) subducted sediments [*Bebout et al.*, 2013; *Elliott*, 2003; *Plank*, 2005; *Plank and Langmuir*, 1998]; and (iii) the serpentinized forearc mantle wedge [*Hattori and Guillot*, 2003; *Savov et al.*, 2007; *Scambelluri and Tonarini*, 2012; *Stern et al.*, 2006; *Straub and Layne*, 2003].

[28] The subducting plate is composed of altered oceanic crust with a thin sediment cover. Pacific sediments and the altered oceanic crust have different Sr-Pb isotopic ratios, FME/aqueous fluid-immobile element ratios, Th/Nb and La/Sm (Figures 6–8) [*Hauff et al.*, 2003; *Kelley et al.*, 2003; *Plank and Langmuir*, 1998], and by combining these differences we can discriminate and estimate the different contributions from downgoing sediments and oceanic crust in SEMFR lavas. The mixing arrays were calculated assuming bulk mixtures. Thus, proportions in these components are maximum proportions, because if a fluid or a melt phase is extracted from these components, the trace element concentrations of the fluid/melt should be higher than the starting concentrations.

[29] Occurrence of a component from subducted Pacific sediments is demonstrated in SEMFR lavas by their BAB-like Th/Nb and La/Sm (Figures 7b, e-f and 8d-e) and a negative Ce anomaly [*Elliott et al.*, 1997] (Figure 5), likely inherited from sediment-melts. Ce anomalies are observed in Mariana sediments [*Plank and Langmuir*, 1998], and during subduction, the sediments transfer their chemical imprint to the lavas [*Elliott et al.*, 1997]. Thus, low Ce/Pb in SEMFR lavas, plotting toward the Pacific sediments (Figure 8c), also reflects a sediment contribution in SEMFR lavas. Contribution of a sediment melt shifts the magma composition toward higher Th/Nb without modifying the Sr-Pb-Nd isotopic ratios relative to its source, resulting in lavas with higher Th/Nb than do the subducted sediment, as seen the Mariana arc lavas (figure 8d). We can thus use an averaged composition of the Mariana arc Th/Nb with the Pb isotopic ratios of the Mariana sediment to estimate the composition of the sediment melt released beneath SEMFR (orange star in Figure 8d). However, mixing between a sediment melt and the SEMFR mantle wedge (orange line in Figure 8d) do not account for the compositional variations seen in SEMFR lavas. Instead, their composition is better explained by mixing between the bulk Mariana sediment and the mantle wedge, demonstrating a small contribution of the sediment melt in SEMFR lavas, and ≤60% sediment melts fluxed the SEMFR mantle wedge (Figures 8d-e). Alternatively, the BAB-like Th/Nb in SEMFR lavas could be inherited from the SEMFR mantle wedge, and it may not reflect the composition of the subduction components released beneath SEMFR.

[30] An aqueous fluid released from the altered oceanic crust can also be seen in SEMFR lavas, as

Geochemistry
Geophysics
Geosystems

G^3

RIBEIRO ET AL.: MANTLE & SUBDUCTION INPUTS BENEATH SEMFR

10.1002/ggge.20244

demonstrated by their elevated Ba/Th, Rb/Th, and Cs/Th, associated with low La/Sm, trending toward the oceanic crust (Figures 7e-f). The crust component is also revealed in the SEMFR Sr-Nd-Pb isotopic ratios that form a linear array from the mantle wedge toward a mixture composed of 35–55% subducted sediments and 45–65% Pacific oceanic crust (Figures 6c–e). ≤60% of this mixture fluxed the SEMFR mantle wedge. In addition, SE SEMFR lavas and NW SEMFR lavas, along with South Mariana arc lavas (13°10'N–11°N, [*Stern et al.*, 2013]), have distinct Pb isotopic compositions, and they plot along two distinct linear arrays. The SE SEMFR lavas plot toward the subducted sediments; while the NW SEMFR lavas and the South Mariana arc lavas trend toward the subducted oceanic crust (Figures 6c–6e), suggesting that the crust component becomes more important away from the trench.

[31] Serpentinized forearc peridotites can also be a source of aqueous fluids in SEMFR lavas. Serpentinites form by hydration of olivine-rich mantle peridotite during shallow dehydration of the subducting plate [*Deschamps et al.*, 2010; *Fryer et al.*, 2006; *Pabst et al.*, 2011; *Pabst et al.*, 2012]. They are stable until ∼ 80–200 km depth [*Evans et al.*, 2013] and they can store large amount of FMEs [*Deschamps et al.*, 2011; *Savov et al.*, 2007]. Forearc serpentinites are dragged down by the subducting plate [*Hattori and Guillot*, 2003; *Savov et al.*, 2007] to release their aqueous fluids into the hot asthenospheric mantle wedge beneath the arc volcanoes [*Hattori and Guillot*, 2003; *Scambelluri and Tonarini*, 2012]. Serpentinized peridotites from the South Chamorro mud seamount in the southern Mariana forearc (13°50N, 146°E) [*Fryer et al.*, 2006; *Savov et al.*, 2007] is a good end-member to demonstrate the role of forearc serpentinites above a shallow subduction zone. The Ba/Th, Cs/Th and Rb/Th of SEMFR lavas and Mariana arc lavas plot along an array from the mantle wedge toward serpentinized forearc peridotite [*Savov et al.*, 2007] (Figures 7c, 7d, and 8a), demonstrating that serpentinite dehydration plays a major role in generating SEMFR and Mariana arc lavas. The serpentinite component becomes increasingly important beneath NE SEMFR, as shown by the highest FME ratios observed in NW SEMFR glassy rinds relative to the SE SEMFR glassy rinds (Figures 7c-d). Plotting Ba/Th against $^{87}Sr/^{86}Sr$ also shows that the compositional variations in SEMFR lavas are explained by mixing between the mantle wedge and an aqueous fluids released from dehydrating a mixture composed of

20–70% forearc serpentinites and 30–80% subducted Pacific crust (Figure 8a). ≤ 40% of this mixture fluxed the SEMFR mantle wedge. Sediments can also dehydrate and contribute to the slab-derived aqueous fluids. When considering a mixture composed of 80–20% serpentinites and sediment (not shown), ≤35% of this aqueous fluid was involved in SEMFR magmagenesis. However, we suspect that the contribution of the Pacific sediments as aqueous fluids is minimal compared to the aqueous fluids released from the oceanic crust and the serpenitinized peridotites, as shown by the FME ratios in Figures 7c–7e.

[32] In summary, SEMFR budgets for Ba, Cs, Rb are controlled by dehydration of subducted oceanic crust and serpentinized forearc mantle wedge; whereas their Th, La, Ce, and Pb budgets are controlled by melting of subducted sediments. Sediments dehydration may also release some aqueous fluids that contribute to a lesser extent to the Cs, Ba, Rb budget relative to the oceanic crust and the forearc mantle wedge. The compositional variations of SEMFR lavas are thus explained by mixing between a BAB-like mantle wedge, aqueous fluids released from dehydrating the downgoing plate and the dragged-down forearc serpentinites, and a sediment melt. Alternatively, occurrence of sediment melt in SEMFR lavas could result from an earlier modification of the SEMFR mantle wedge. Contribution of the crust and serpentinite components in Ba, Cs, and Rb budgets becomes more important away from the trench.

5.3. Tracking Mantle and Subduction Flows

[33] Compositional evolution of the subduction and mantle components can be mapped beneath the SE Mariana forearc by using elemental ratios [*Pearce et al.*, 2005]. We use Ba/Th, Rb/Th, and Cs/Th proxies to illustrate the release and quantities of aqueous fluids, Th/Nb for the sediment melt, and Nb/Yb for the mantle depletion and to infer mantle flow [*Pearce and Stern*, 2006; *Pearce et al.*, 2005] along SEMFR.

[34] Ba/Th and Th/Nb in South Mariana arc-backarc basin lavas increase from MGR toward the active arc volcanoes (Figures 9a,c), demonstrating that aqueous fluids and deep sediment melt are mostly captured by the magmatic arc volcanoes [*Pearce et al.*, 2005]. The southern termination of the Mariana Trough, where the spreading center almost intersects with the active arc
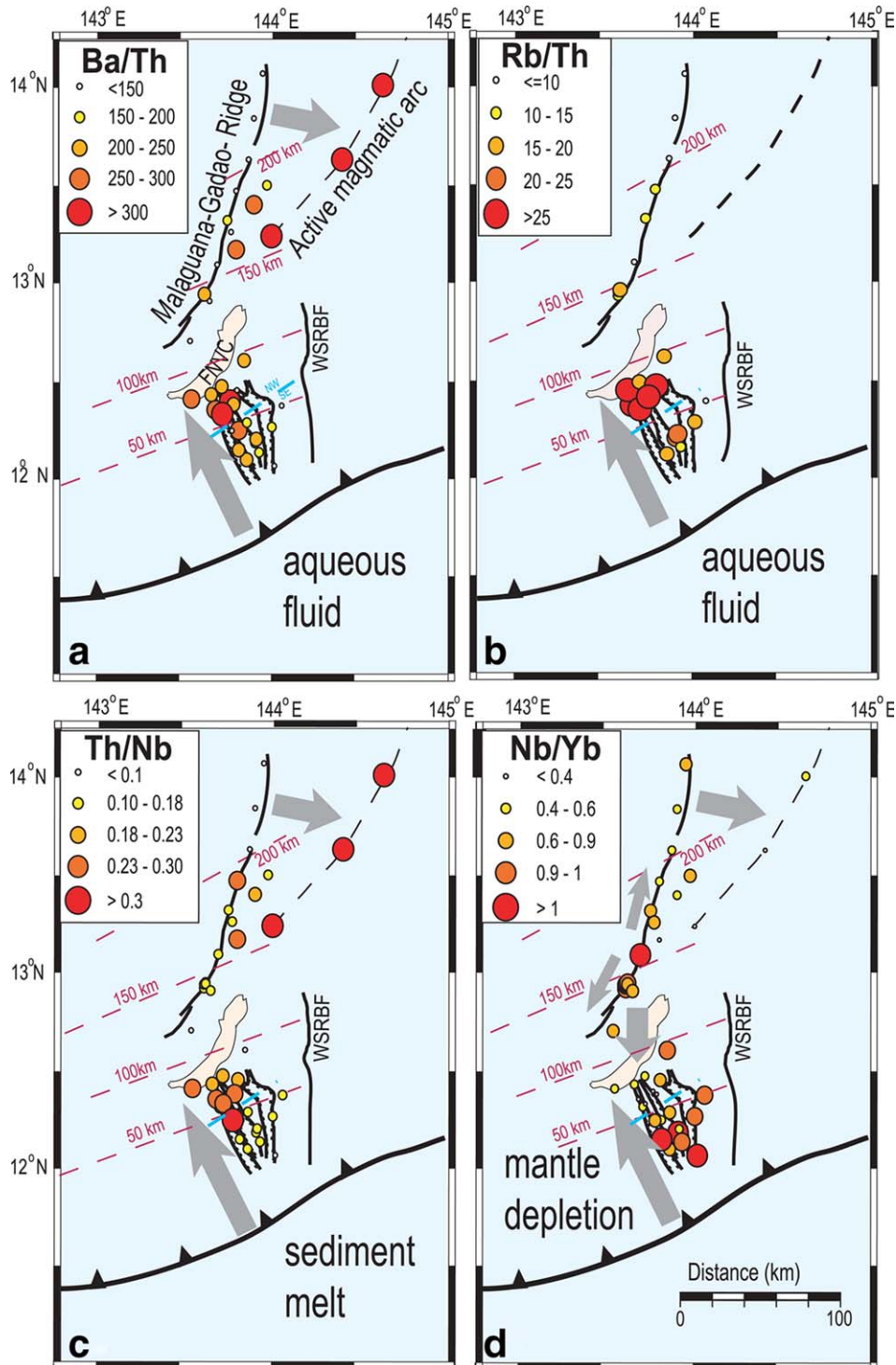
Figure 9. Geochemical maps of the subduction and mantle components in the SE Mariana convergent margin, after [*Pearce et al.*, 2005]. (a) Ba/Th and (b) Rb/Th, are proxies mapping the aqueous fluid; and (c) Th/Nb ratio maps sediment melt. Cs/Th is not shown but shows similar variation to Rb/Th. The subduction components along SEMFR increase toward the Fina-Nagu volcanic arc chain (FNVC), as denoted by the grey arrow. (d) Nb/Yb tracks mantle fertility and mantle flow. Along SEMFR, Nb/Yb increases toward the trench, indicating that depletion increased away from the trench. This suggests that, from 3.7 to 2.7 Ma, the mantle flowed from the trench toward the arc volcanoes, as illustrated by the long grey arrow. The shorter grey arrows show modern, inferred mantle flow beneath MGR. See text for details.
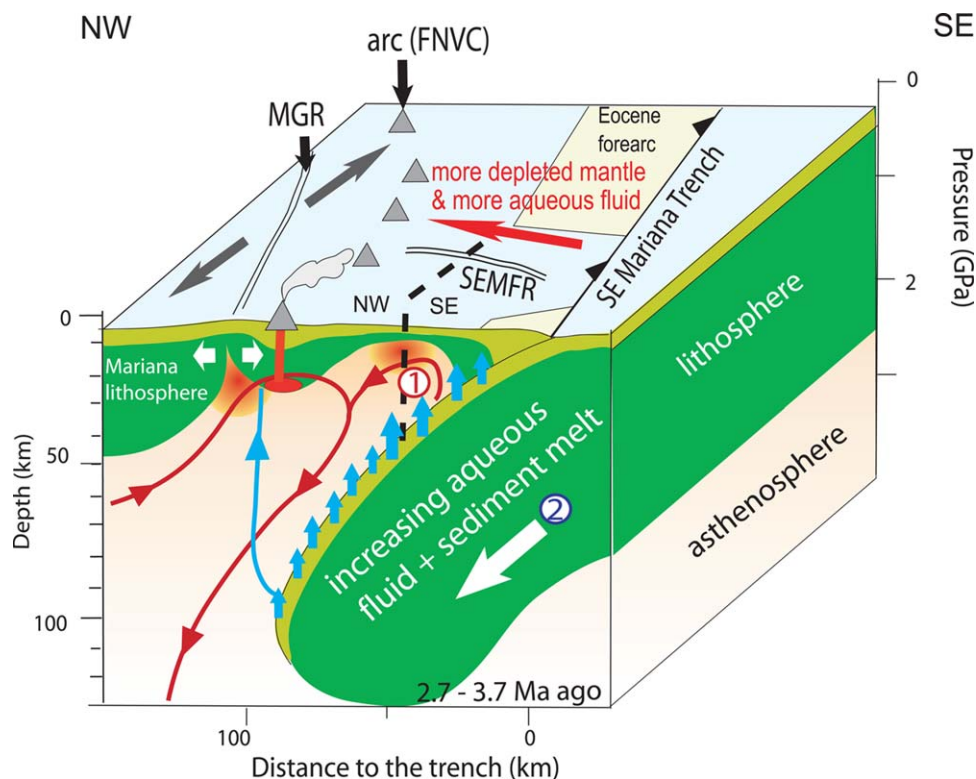
Figure 10. 3D model of magmagenesis for SEMFR lavas. Mantle depletion increases away from the trench, suggesting that new mantle input flowed beneath SEMFR toward the arc (1). The aqueous fluid and the sediment melt increase toward the arc volcanoes (2). The grey arrow shows the opening of MGR. The red arrow shows the mantle flow and the subduction components along SEMFR.

volcanoes south of 13°N, has intermediate Ba/Th and Th/Nb, between the values of the arc and the backarc basin spreading center. This result is consistent with the interpretations of [*Becker et al.*, 2010; *Fryer*, 1993; *Stern et al.*, 2013], suggesting that the southernmost MGR, localized at ~150 km above the Wadati-Benioff zone [*Becker*, 2005; *Fryer et al.*, 1998], captures the aqueous fluids and sediment melt usually released beneath arc volcanoes. Along SEMFR, the proxies Ba/Th, Cs/Th, Rb/Th, and Th/Nb increase NE toward the arc volcanoes (Figures 9a–c), demonstrating that aqueous fluid and sediment melt contributions both increase with slab depth. This observation, in agreement with [*Hulme et al.*, 2010], demonstrates that the composition of the aqueous fluids is controlled by the P-T path of the subducting slab and the breakdown of Rb-Cs-Ba-rich minerals (such as barite [*Plank and Langmuir*, 1998]; phengite [*Zack et al.*, 2001], and serpentinite [*Pabst et al.*, 2012; *Savov et al.*, 2007; *Savov et al.*, 2005]). Beneath SEMFR, slab-derived inputs of Ba, Cs and Rb are the greatest between ~ 50 and 100 km slab depth (Figures 9a–c; and 10), suggesting that

Rb-Cs-Ba-rich minerals released their aqueous fluids deeper than beneath the outer forearc (Figure 1) [*Evans et al.*, 2013; *Pabst et al.*, 2012]. These results are consistent with the numerical modeling of [*Van Keken et al.*, 2011; *Wada et al.*, 2008], with the chemical variations of arc lavas of [*Ruscitto et al.*, 2012], and with the studies of metamorphic rocks [*Bebout et al.*, 1999; *Bebout et al.*, 2013; *Pabst et al.*, 2012], which showed that at cooler subduction zones, such as the Mariana convergent margin, the subducting plate retains much of its aqueous fluids to release them beneath the arc volcanoes. In contrast, warmer slabs mostly dehydrate beneath the forearc (<80 km slab depth) and the aqueous slab-derived fluids participate to arc magmatism to a lesser extent [*Ruscitto et al.*, 2012; *Van Keken et al.*, 2011].

[35] The Nb/Yb ratio (Figure 9d) varies along and across the backarc basin spreading center. Along MGR, Nb/Yb is the highest around 13°10'N, where a magma chamber was identified [*Becker et al.*, 2010]. Across MGR, Nb/Yb decreases from the backarc basin spreading center toward the

South Mariana arc volcanoes, demonstrating that sub-arc mantle is more depleted than the sub-BAB mantle, and the mantle flows from MGR toward the arc volcanoes [*Pearce and Stern*, 2006; *Pearce et al.*, 2005]. Such variations in Nb/Yb suggest that the forearc mantle should be more depleted than the arc mantle (Figure 1). However, in SEMFR lavas, Nb/Yb decreases toward the arc volcanoes (FNVC), reflecting a more depleted mantle source away from the trench. This result are consistent with higher shallow subduction input toward the NW, resulting in higher degrees of mantle melting away from the trench. Nb/Yb variations along SEMFR also suggest that new undepleted mantle flowed toward the SE Mariana trench when SEMFR formed. This new input of asthenospheric mantle suggests that the Pacific mantle flowed around the N-S southernmost Mariana slab edge beneath the WSRBF [*Fryer et al.*, 2003; *Gvirtzman and Stern*, 2004] and infiltrated the SEMFR mantle wedge. Hf-Nd-Pb isotopic ratios have been used to demonstrate the Indian origin of the Mariana mantle [*Hickey-Vargas et al.*, 2006; *Pearce et al.*, 1999; *Woodhead et al.*, 2012], and such ratios could be used to discriminate the Indian or the Pacific origin of the SEMFR mantle. Indeed, if the Pacific mantle flowed beneath SEMFR, the SE SEMFR mantle would have a Pacific origin or it would be composed of a mixture between an Indian and a Pacific mantle, evolving toward the Indian end-member away from the trench. To test that hypothesis, the Hf isotopic composition of SEMFR lavas needs to be analyzed.

6. Conclusions

[36] The SE Mariana forearc lithosphere stretched to accommodate opening of the southernmost Mariana Trough, forming SEMFR 3.7–2.7 Ma ago. The presence of young basalts in the SE Mariana intraoceanic arc provides an opportunity to investigate compositional evolution of the shallow mantle and subduction processes unusually close to the trench and above a very shallow subduction zone. SEMFR lavas did not form from a strongly depleted, forearc mantle source, as expected. Instead, they formed from a less depleted, BAB-like mantle source that flowed from the trench toward the arc volcanoes, suggesting that new input of less depleted mantle flowed from near the trench toward the arc (Figure 10), counter to the flow expected beneath convergent plate margins. Mantle beneath SEMFR captured aqueous fluids released

from the altered oceanic crust and the dragged-down forearc serpentinites, and the chemical imprint of the fluids is reflected in the composition of melts that they generated. These aqueous, slab-derived fluids are more enriched in Cs and Rb, and slightly more enriched in Ba, than are the deeper fluids released beneath arc volcanoes and the back-arc spreading center, suggesting that SEMFR mantle trapped the aqueous fluids released from the shallow part of the subducting plate. Aqueous fluids derive from dehydrating ≤40% the downgoing plate and the serpentinized forearc mantle (Figure 10). Another surprising result is that SEMFR melts, including SE SEMFR lavas (Figure 7b), show a melt component released from subducted sediments (demonstrated by BAB-like Th/Nb and La/Sm), which is generally thought to be released much deeper (≥ 100 km) [*Johnson and Plank*, 1999; *Pearce et al.*, 2005]. Occurrence of a deep BAB-like, sediment melt component in SEMFR lavas could be inherited from an earlier modification of their mantle source and may not reflect shallow subduction zone processes. Finally, the absence of a strong subduction component in SE SEMFR lavas indicates that aqueous fluids and sediment melts are mostly released at 50–100 km slab depth. These new geochemical datasets led us to the interpretation that the Cs-Ba-Rb-rich minerals (phengite, serpentinite, barite) from the subducting slab mostly broke down beneath the arc volcanoes in the Mariana convergent margin, consistent with the modeling of [*Van Keken et al.*, 2011; *Wada et al.*, 2008] and with the chemical studies of arc lavas [*Ruscitto et al.*, 2012] and metamorphic rocks [*Bebout et al.*, 2013; *Hattori and Guillot*, 2007; *Pabst et al.*, 2012; *Scambelluri and Tonarini*, 2012].

Acknowledgments

References

Arculus, R. J. (2003), Use and abuse of the terms calcalkaline and calcalkalic, *J. Petrol.*, *44*, 929–935.

Bebout, G. E. (2007), Metamorphic chemical geodynamics of subduction zones, *Earth Planet. Sci. Lett.*, *260*, 373–393.

Bebout, G. E., A. E. Bebout, and C. M. Graham (2007), Cycling of B, Li, and LILE (K, Cs, Rb, Ba, Sr) into subduction zones: SIMS evidence from micas in high-P/T metasedimentary rocks, *Chem. Geol.*, *239*, 284–304.

Bebout, G. E., J. G. Ryan, W. P. Leeman, and A. E. Bebout (1999), Fractionation of trace elements by subduction-zone

metamorphism—Effect of convergent-margin thermal evolution, *Earth Planet. Sci. Lett.*, *171*, 63–81.

Bebout, G. E., P. Agard, K. Kobayashi, T. Moriguti, and E. Nakamura (2013), Devolatilization history and trace element mobility in deeply subducted sedimentary rocks: Evidence from Western Alps HP/UHP suites, *Chem. Geol.*, *342*, 1–20.

Becker, N. C. (2005), Recent volcanic and tectonic evolution of the southern Mariana arc, PhD Dissertation thesis, University of Hawai'i, Hawai', pp. 166.

Becker, N. C., P. Fryer, and G. F. Moore (2010), Malaguana-Gadao Ridge: Identification and implications of a magma chamber reflector in the southern Mariana Trough, *Geochem. Geophys. Geosyst.*, *11*, Q04X13, doi:10.1029/2009GC002719.

Bloomer, S. H., and J. W. Hawkins (1983), *Gabbroic and ultramafic rocks from the Mariana Trench: An island arc ophiolite, in The Tectonic and Geologic Evolution of Southeast Asian Seas and Islands: Part 2*, edited by D. E. Hayes, pp. 294–317, Geophysical Monograph Series, Washington, D.C.

Chauvel, C., and J. Blichert-Toft (2001), A hafnium isotope and trace element perspective on melting of the depleted mantle, *Earth Planet. Sci. Lett.*, *190*, 137–151.

Class, C., D. M. Miller, S. L. Goldstein, and C. H. Langmuir (2000), Distinguishing melt and fluid subduction components in Umnak Volcanics, Aleutian Arc, *Geochem. Geophys. Geosyst.*, *1*, 1–30.

Deschamps, F., S. Guillot, M. Godard, M. Andreani, and K. Hattori (2011), Serpentinites act as sponges for fluid-mobile elements in abyssal and subduction zone environments, *Terra Nova*, *23*, 171–178.

Deschamps, F., S. Guillot, M. Godard, C. Chauvel, M. Andreani, and K. Hattori (2010), In situ characterization of serpentinites from forearc mantle wedges: Timing of serpentinization and behavior of fluid-mobile elements in subduction zones, *Chem. Geol.*, *269*, 262–277.

Elliott, T. R. (2003), *Tracers of the slab, in Inside the Subduction Factory*, edited by J. Eiler, pp. 23–45, Geophysical Monograph Series, Washington, D.C.

Elliott, T. R., T. Plank, A. Zindler, W. White, and B. Bourdon (1997), Element transport from slab to volcanic front at the Mariana arc, *J. Geophys. Res.*, *B102*, 14,991–15,019.

Escrig, S., A. Bézos, S. L. Goldstein, C. H. Langmuir, and P. J. Michael (2009), Mantle source variations beneath the Eastern Lau spreading center and the nature of subduction components in the Lau basin–Tonga arc system, *Geochem. Geophys. Geosyst.*, *10*, Q04014, doi:10.01029/02008gc002281.

Evans, B. W., K. Hattori, and A. Baronnet (2013), Serpentinite: What, why, where?, *Elements*, *9*, 99–106.

Fryer, P. (1993), The relationship between tectonic deformation, volcanism, and fluid venting in the southeastern Mariana convergent plate margin, *Proceedings of JAMSTEC, Symposium on Deep Sea Res.*, *9*, 161–179.

Fryer, P., J. Gharib, K. Ross, I. Savov, and M. J. Mottl (2006), Variability in serpentinite mudflow mechanisms and sources: ODP drilling results on Mariana forearc seamounts, *Geochem. Geophys. Geosyst.*, *7*, Q08014, doi:08010.01029/02005gc001201.

Fryer, P., M. Mottl, L. Johnson, J. Haggerty, S. Phipps, and H. Maekawa (1995), *Serpentine bodies in the forearcs of western Pacific convergent margins: Origin and associated fluids, in Active Margins and Marginal Basins of the Western Pacific*, edited by B. Taylor and J. Natland, pp. 259–279, AGU, Washington, D.C.

Fryer, P., N. Becker, B. Appelgate, F. Martinez, M. Edwards, and G. Fryer (2003), Why is the Challenger Deep so deep?, *Earth Planet. Sci. Lett.*, *211*, 259–269.

Fryer, P., H. Fujimoto, M. Sekine, L. Johnson, J. Kasahara, H. Masuda, T. Gamo, T. Ishii, M. Ariyoshi, and K. Fujioka (1998), Volcanoes of the southwestern extension of the active Mariana island arc: New swath-mapping and geochemical studies, *Isl. Arc*, *7*, 596–607.

Gamo, T., et al. (2004), Discovery of a new hydrothermal venting site in the southernmost Mariana Arc: Al-rich hydrothermal plumes and white smoker activity associated with biogenic methane, *Geochem. J.*, *38*, 527–534.

Gardner, J. V. (2006), *Law of the sea Cruise to map the western insular margin and 2500-m isobath of Guam and the northern Mariana islands, Cruise Report*, p. *45*, University of New Hampshire (UNH), Durham, NH.

Gardner, J. V. (2007), *U.S. Law of the sea Cruise to map the western insular margin and 2500-m isobath of Guam and the northern mariana islands, Cruise Report*, p. *37*, University of New Hampshire (UNH), Durham, NH.

Gardner, J. V. (2010), *U.S. Law of the sea Cruises to map sections of the Mariana trench and the eastern and southern insular margins of Guam and the northern Mariana islands, Cruise Report*, p. *82*, University of New Hampshire (UNH), Durham, NH.

Gribble, R. F., R. J. Stern, S. Newman, S. H. Bloomer, and T. O'Hearn (1998), Chemical and isotopic composition of Lavas from the northern Mariana trough: Implications for magmagenesis in back-arc basins, *J. Petrol.*, *39*, 125–154.

Gribble, R. F., R. J. Stern, S. H. Bloomer, D. Stüben, T. O'Hearn, and S. Newman (1996), MORB mantle and subduction components interact to generate basalts in the southern Mariana Trough back-arc basin, *Geochim. Cosmochim. Acta*, *60*, 2153–2166.

Grove, T. L., R. J. Kinzler, and W. B. Bryan (1992), *Fractionation of mid-ocean ridge basalt (MORB), in Mantle Flow and Melt Generation at Mid-Ocean Ridges*, edited by J. P. Morgan, D. K. Blackman, and J. M. Sinton, pp. 281–310, Geophysical Monograph Series, Washington, D.C.

Gvirtzman, Z., and R. J. Stern (2004), Bathymetry of Mariana trench-arc system and formation of the Challenger Deep as a consequence of weak plate coupling, *Tectonics*, *23*, TC2011, doi:2010.1029/2003tc001581.

Hacker, B. R. (2008), H2O subduction beyond arcs, *Geochem. Geophys. Geosyst.*, *9*, Q03001, doi:03010.01029/02007gc001707.

Hart, S. R. (1969), K, Rb, Cs contents and K/Rb, K/Cs ratios of fresh and altered submarine basalts, *Earth Planet. Sci. Lett.*, *6*, 295–303.

Hattori, K. H., and S. Guillot (2003), Volcanic fronts form as a consequence of serpentinite dehydration in the forearc mantle wedge, *Geology*, *31*, 525–528.

Hattori, K. H., and S. Guillot (2007), Geochemical character of serpentinites associated with high- to ultrahigh-pressure metamorphic rocks in the Alps, Cuba, and the Himalayas: Recycling of elements in subduction zones, *Geochem. Geophys. Geosyst.*, *8*, Q09010, doi:09010.01029/02007gc001594.

Hauff, F., K. Hoernle, and A. Schmidt (2003), Sr-Nd-Pb composition of Mesozoic Pacific oceanic crust (Site 1149 and 801, ODP Leg 185): Implications for alteration of ocean crust and the input into the Izu-Bonin-Mariana subduction system, *Geochem. Geophys. Geosyst.*, *4*, 8913, doi:8910.1029/2002gc000421.

Hawkins, J. W., P. F. Lonsdale, J. D. Macdougall, and A. M. Volpe (1990), Petrology of the axial ridge of the Mariana

Trough backarc spreading center, *Earth Planet. Sci. Lett.*, *100*, 226–250.

Hickey-Vargas, R., I. P. Savov, M. Bizimis, T. Ishii, and K. Fujioka (2006), *Origin of diverse geochemical signatures in igneous rocks from the West Philippine Basin: Implications for tectonic models, in Back-Arc Spreading Systems: Geological, Biological, Chemical, and Physical Interactions*, edited by D. M. Christie et al., pp. 287–303, Geophysical monograph Series, Washington, D.C.

Hulme, S. M., C. G. Wheat, P. Fryer, and M. J. Mottl (2010), Pore water chemistry of the Mariana serpentinite mud volcanoes: A window to the seismogenic zone, *Geochem. Geophys. Geosyst.*, *11*, Q01X09, doi:10.1029/2009gc002674.

Ikeda, Y., K. Nagao, R. J. Stern, M. Yuasa, and S. Newman (1998), Noble gases in pillow basalt glasses from the northern Mariana Trough back-arc basin, *Isl. Arc*, *7*, 471–478.

Ishizuka, O., M. Yuasa, R. N. Taylor, and I. Sakamoto (2009), Two contrasting magmatic types coexist after the cessation of back-arc spreading, *Chem. Geol.*, *266*, 274–296.

Jenner, F. E., and H. S. C. O'Neill (2012), Analysis of 60 elements in 616 ocean floor basaltic glasses, *Geochem. Geophys. Geosyst.*, *13*, Q02005, doi:02010.01029/02011gc004009.

Jochum, K. P., and S. P. Verma (1996), Extreme enrichment of Sb, Tl and other trace elements in altered MORB, *Chem. Geol.*, *130*, 289–299.

Johnson, M. C., and T. Plank (1999), Dehydration and melting experiments constrain the fate of subducted sediments, *Geochem. Geophys. Geosyst.*, *1*, 1–26.

Kakegawa, T., M. Utsumi, and K. Marumo (2008), Geochemistry of sulfide chimneys and basement pillow lavas at the southern Mariana trough (12.55°N and12.58°N), *Resour. Geol.*, *58*, 249–266.

Kato, T., J. Beavan, T. Matsushima, Y. Kotake, J. T. Camacho, and S. Nakao (2003), Geodetic evidence of back arc spreading in the Mariana Trough, *Geophys. Res. Lett.*, *30*, 1625, doi:1610.1029/2002GL016757.

Kelley, K. A., and E. Cottrell (2009), Water and the oxidation state of subduction zone magmas, *Science*, *325*, 605–607.

Kelley, K. A., T. Plank, J. Ludden, and H. Staudigel (2003), Composition of altered oceanic crust at ODP sites 801 and 1149, *Geochem. Geophys. Geosyst.*, *4*, 8910, doi:8910.1029/2002GC000435.

Kelley, K. A., T. Plank, T. L. Grove, E. M. Stolper, S. Newman, and E. H. Hauri (2006), Mantle melting as a function of water content beneath back-arc basins, *J. Geophys. Res.*, *111*, B09208, doi:09210.01029/02005jb003732.

Kelley, K. A., T. Plank, S. Newman, E. M. Stolper, T. L. Grove, S. W. Parman, and E. H. Hauri (2010), Mantle melting as a function of water content beneath the Mariana arc, *J. Petrol.*, *51*, 1711–1738.

Kent, A. J. R., and T. R. Elliott (2002), Melt inclusions from Marianas arc lavas: Implications for the composition and formation of island arc magmas, *Chem. Geol.*, *183*, 263–286.

Kimura, J.-I., A. Kent, M. C. Rowe, M. Katakuse, F. Nakano, B. R. Hacker, P. E. Van Keken, H. Kawabata, and R. J. Stern (2010), Origin of cross-chain geochemical variation in Quaternary lavas from the northern Izu arc: Using a quantitative mass balance approach to identify mantle sources and mantle wedge processes, *Geochem. Geophys. Geosyst.*, *11*, Q10011, doi:10010.11029/12010gc003050.

Klein, E. M., and C. H. Langmuir (1987), Global correlations of ocean ridge basalt chemistry with axial depth and crustal thickness, *J. Geophys. Res.*, *92*, 8089–8115.

Langmuir, C. H., A. Bezos, S. Escrig, and S. W. Parman (2006), *Chemical systematics and hydrous melting of the mantle in back-arc basins, in Back-Arc Spreading Systems: Geological, Biological, Chemical, and Physical Interactions*, edited by D. M. Christie et al., pp. 87–146, Geophysical Monograph Series, Washington, D.C.

Le Bas, M. J. (2000), IUGS reclassification of the high-Mg and Picritic volcanic rocks, *J. Petrol.*, *41*, 1467–1470.

Lee, C.-T. A., P. Luffi, T. Plank, H. Dalton, and W. P. Leeman (2009), Constraints on the depths and temperatures of basaltic magma generation on Earth and other terrestrial planets using new thermobarometers for mafic magmas, *Earth Planet. Sci. Lett.*, *279*, 20–33.

Manning, C. E. (2004), The chemistry of subduction-zone fluids, *Earth Planet. Sci. Lett.*, *223*, 1–16.

McCulloch, M. T., and J. A. Gamble (1991), Geochemical and geodynamical constraints on subduction zone magmatism, *Earth Planet. Sci. Lett.*, *102*, 358–374.

Michibayashi, K., Y. Ohara, R. J. Stern, P. Fryer, J.-I. Kimura, M. Tasaka, Y. Harigane, and T. Ishii (2009), Peridotites from a ductile shear zone within back-arc lithospheric mantle, southern Mariana Trench: Results of a Shinkai 6500 dive, *Geochem. Geophys. Geosyst.*, *10*, Q05X06, doi:10.1029/2008GC002197.

Miller, M. S., A. Gorbatov, and B. L. N. Kennett (2006), Three-dimensional visualization of a near-vertical slab tear beneath the southern Mariana arc, *Geochem. Geophys. Geosyst.*, *7*, Q06012, doi:06010.01029/02005gc001110.

Miyashiro, A. (1974), Volcanic rock series in island arcs and active continental margins, *Am. J. Sci.*, *274*, 321–355.

Ohara, Y., and T. Ishii (1998), Peridotites from the southern Mariana forearc: Heterogeneous fluid supply in mantle wedge, *Isl. Arc*, *7*, 541–558.

Ohara, Y., R. J. Stern, T. Ishii, H. Yurimoto, and T. Yamazaki (2002), Peridotites from the Mariana trough: First look at the mantle beneath an active back-arc basin, *Contrib. Mineral. Petrol.*, *143*, 1–18.

Pabst, S., T. Z. Zack, I. P. Savov, T. Ludwig, D. Rost, and E. P. Vicenzi (2011), Evidence for boron incorporation into the serpentine crystal structure, *Am. Mineral.*, *96*, 1112–1119.

Pabst, S., T. Zack, I. P. Savov, T. Ludwig, D. Rost, S. Tonarini, and E. P. Vicenzi (2012), The fate of subducted oceanic slabs in the shallow mantle: Insights from boron isotopes and light element composition of metasomatized blueschists from the Mariana forearc, *Lithos*, *132–133*, 162–179.

Parkinson, I. J., and J. A. Pearce (1998), Peridotites from the Izu–Bonin–Mariana forearc (ODP Leg 125): Evidence for mantle melting and melt–mantle interaction in a supra-subduction zone setting, *J. Petrol.*, *39*, 1577–1618.

Pearce, J. A. (2008), Geochemical fingerprintring of oceanic basalts with applications to ophiolite classification and the search for Archean oceanic crust, *Lithos*, *100*, 14–48.

Pearce, J. A., and R. J. Stern (2006), *Origin of Back-Arc basin magmas: Trace element and isotope perspectives, in Back-Arc Spreading Systems: Geological, Biological, Chemical, and Physical Interactions*, edited by D. M. Christie et al., pp. 63–86, Geophysical Monograph Series, Washington, D.C.

Pearce, J. A., P. D. Kempton, G. M. Nowell, and S. R. Noble (1999), Hf-Nd element and isotope perspective on the nature and provenance of mantle and subduction components in western Pacific Arc-basin systems, *J. Petrol.*, *40*, 1579–1611.

Pearce, J. A., R. J. Stern, S. H. Bloomer, and P. Fryer (2005), Geochemical mapping of the Mariana arc-basin system: Implications for the nature and distribution of subduction components, *Geochem. Geophys. Geosyst.*, *6*, Q07006, doi:07010.01029/02004GC000895.

Peccerillo, A., and S. R. Taylor (1976), Geochemistry of Eocene calcalkaline volcanic rocks from the Kastamonu area, Northern Turkey, *Contrib. Mineral. Petrol.*, *58*, 63–81.

Plank, T. (2005), Constraints from thorium/lanthanum on sediment recycling at subduction zones and the evolution of the continents, *J. Petrol.*, *46*, 921–944.

Plank, T., and C. H. Langmuir (1998), The chemical composition of subducting sediment and its consequences for the crust and mantle, *Chem. Geol.*, *145*, 325–394.

Reagan, M. K., et al. (2010), Fore-arc basalts and subduction initiation in the Izu-Bonin-Mariana system, *Geochem. Geophys. Geosyst.*, *11*, Q03X12, doi:10.1029/2009GC002871.

Ribeiro, J., et al., (2013), Geodynamic evolution of a forearc rift in the southernmost Mariana Arc, *Island Arc.*, doi:10.1111/iar.12039.

Ruscitto, D. M., P. J. Wallace, L. B. Cooper, and T. Plank (2012), Global variations in H2O/Ce: 2. Relationships to arc magma geochemistry and volatile fluxes, *Geochem. Geophys. Geosyst.*, *13*, Q03025, doi:03010.01029/02011gc003887.

Ryan, J. G., J. Morris, F. Tera, W. P. Leeman, and A. Tsvetkov (1995), Cross-arc geochemical variations in the Kurile arc as a function of slab depth, *Science*, *270*, 625–627.

Salters, V. J. M., and A. Stracke (2004), Composition of the depleted mantle, *Geochem. Geophys. Geosyst.*, *5*, Q05B07, doi:10.1029/2003GC000597.

Sato, H., and T. Ishii (2011), *Petrology and mineralogy of mantle peridotites from the southern Marianas, in Accretionary Prisms and Convergent Margin Tectonics in the Northwest Pacific Basin*, edited by Y. Ogawa, R. Anma, and Y. Dilek, pp. 129–147, Springer, Houten, Netherlands.

Savov, I. P., J. G. Ryan, M. D' Antonio, and P. Fryer (2007), Shallow slab fluid release across and along the Mariana arc-basin system: Insights from geochemistry of serpentinized peridotites from the Mariana fore arc, *J. Geophys. Res.*, *112*, B09205, doi:09210.01029/02006JB004749.

Savov, I. P., J. G. Ryan, M. D' Antonio, K. Kelley, and P. Mattie (2005), Geochemistry of serpentinized peridotites from the Mariana forearc conical seamount, ODP Leg 125: Implications for the elemental recycling at subduction zones, *Geochem. Geophys. Geosyst.*, *6*, Q04J15, doi:10.1029/2004GC000777.

Scambelluri, M., and S. Tonarini (2012), Boron isotope evidence for shallow fluid transfer across subduction zones by serpentinized mantle, *Geology*, *40*, 907–910.

Schmidt, M., and S. Poli (1998), Experimentally based water budgets for dehydrating slabs and consequences for magma generation, *Earth Planet. Sci. Lett.*, *163*, 361–379.

Shaw, A. M., E. H. Hauri, T. P. Fischer, D. R. Hilton, and K. A. Kelley (2008), Hydrogen isotopes in Mariana arc melt inclusions: Implications for subduction dehydration and the deep-Earth water cycle, *Earth Planet. Sci. Lett.*, *275*, 138–145.

Shervais, J. W. (1982), Ti-V plots and the petrogenesis of modern and ophiolitic lavas, *Earth Planet. Sci. Lett.*, *59*, 101–118.

Sisson, T. W., and T. L. Grove (1993), Experimental investigations of the role of H2O in calc-alkaline differentiation and subduction zone magmatism, *Contrib. Mineral. Petrol.*, *113*, 143–166.

Smith, W. H. F., and P. Wessel (1990), Gridding with continuous curvature splines in tension, *Geophysics*, *55*, 293–305.

Stern, R. J. (2002), Subduction zones, *Rev. Geophys.*, *40*, 37, doi:10.1029/2001RG000108.

Stern, R. J., E. Kohut, S. H. Bloomer, M. Leybourne, M. Fouch, and J. Vervoort (2006), Subduction factory processes beneath the Guguan cross-chain, Mariana Arc: No role for sediments, are serpentinites important?, *Contrib. Mineral. Petrol.*, *151*, 202–221.

Stern, R. J., Y. Tamura, H. Masuda, P. Fryer, F. Martinez, O. Ishizuka, and S. H. Bloomer (2013), How the Mariana volcanic arc ends in the south, *Isl. Arc*, *22*, 133–148.

Straub, S. M., and G. D. Layne (2003), Decoupling of fluids and fluid-mobile elements during shallow subduction: Evidence from halogen-rich andesite melt inclusions from the Izu arc volcanic front, *Geochem. Geophys. Geosyst.*, *4*, 9004, doi:9010.1029/2002gc000349.

Sun, S. S., and W. F. McDonough (1989), *Chemical and isotopic systemics of ocean basalt: Implications for mantle composition and processes, in Magmatism in the Ocean Basins*, edited by A. D. Saunders and M. J. Norry, pp. 313–345, Geological Society of London, Special publications, London.

Taylor, B., and F. Martinez (2003), Back-arc basin basalt systematics, *Earth Planet. Sci. Lett.*, *210*, 481–497.

Todt, W., R. Cliff, A. Hanser, and A. Hofmann (1996), *Evaluation of a 202Pb – 205Pb double spike for high – precision lead isotope analysis, in Earth Processes: Reading the Isotopic Code*, edited by A. Basu and S. Hart, pp. 429–437, Geophysical Monograph Series, Washington, D.C.

Van Keken, P. E., B. R. Hacker, E. M. Syracuse, and G. A. Abers (2011), Subduction factory: 4. Depth-dependent flux of H2O from subducting slabs worldwide, *J. Geophys. Res. Solid Earth*, *116*, B01401, doi:01410.01029/02010jb007922.

Volpe, A. M., J. Douglas Macdougall, and J. W. Hawkins (1987), Mariana trough basalts (MTB): Trace element and SrNd isotopic evidence for mixing between MORB-like and Arc-like melts, *Earth Planet. Sci. Lett.*, *82*, 241–254.

Volpe, A. M., J. Douglas Macdougall, G. W. Lugmair, J. W. Hawkins, and P. F. Lonsdale (1990), Fine-scale isotopic variation in Mariana trough basalts: Evidence for heterogeneity and a recycled component in backarc basin mantle, *Earth Planet. Sci. Lett.*, *100*, 251–264.

Wada, I., C. A. Rychert, and K. Wang (2011), Sharp thermal transition in the forearc mantle wedge as a consequence of nonlinear mantle wedge flow, *Geophys. Res. Lett.*, *38*, L13308, doi:13310.11029/12011gl047705.

Wada, I., K. Wang, J. He, and R. D. Hyndman (2008), Weakening of the subduction interface and its effects on surface heat flow, slab dehydration, and mantle wedge serpentinization, *J. Geophys. Res. Solid Earth*, *113*, B04402, doi:10.1029/2007JB005190.

Wade, J. A., et al. (2005), The may 2003 eruption of Anatahan volcano, Mariana Islands: Geochemical evolution of a silicic island-arc volcano, *J. Volcanol. Geoth. Res.*, *146*, 139–170.

Wessel, P., and W. H. F. Smith (1995), *New version of the generic mapping tools released, EOS Trans*. AGU, *76*, 329.

Wessel, P., and W. H. F. Smith (1998), New, improved version of generic mapping tools released, in EOS Transactions American Geophysical Union, 79, 579, Washington, D.C.

Woodhead, J. D. (1989), Geochemistry of the Mariana arc (Western Pacific): Source composition and processes, *Chem. Geol.*, *76*, 1–24.

Woodhead, J. D., R. J. Stern, J. A. Pearce, J. M. Hergt, and J. Vervoort (2012), Hf-Nd isotope variation in Mariana Trough basalts: The importance of "ambient mantle" in the interpretation of subduction zone magmas, *Geology*, *40*, 539–542.

Zack, T., T. Rivers, and S. Foley (2001), Cs-Rb-Ba systematics in phengite and amphibole: An assessment of fluid mobility at 2.0 GPa in eclogites from Trescolmen, Central Alps, *Contrib. Mineral. Petrol.*, *140*, 651–669.